

Chapter 7

Effect of NO_x on Secondary Organic Aerosol (SOA) Formation from Photooxidation of Terpenes*

*This chapter is prepared for journal submission as “Effect of NO_x on secondary organic aerosol (SOA) formation from photooxidation of terpenes” by N. L. Ng, P. S. Chhabra, A. W. H. Chan, J. D. Surratt, J. H. Kroll, A. J. Kwan, D. C. McCabe, P. O. Wennberg, A. Sorooshian, S. M. Murphy, N. F. Dalleska, R. C. Flagan, and J. H. Seinfeld.

7.1 Abstract

Secondary organic aerosol (SOA) formation from the photooxidation of one monoterpene (α -pinene) and two sesquiterpenes (longifolene and aromadendrene) is investigated in the Caltech environmental chambers. By performing photooxidation experiments under varying NO_x conditions, the effect of NO_x on SOA formation for these biogenic hydrocarbons is evaluated. The NO_x dependence of α -pinene SOA formation follows the same trend as that of isoprene (Kroll et al., 2006), in which SOA yield (defined as the ratio of the mass of organic aerosol formed to the mass of parent hydrocarbon reacted) decreases as NO_x level increases. The NO_x dependence of SOA yield for the sesquiterpenes, longifolene and aromadendrene, however, differs from that determined for isoprene and α -pinene; the aerosol yield under high- NO_x conditions substantially exceeds that under low- NO_x conditions. The reversal of the NO_x dependence of SOA formation for the sesquiterpenes is consistent with formation of relatively nonvolatile organic nitrates, and/or the isomerization of large alkoxy radicals that leads to less volatile products. Analysis of the aerosol chemical composition for longifolene confirms the presence of organic nitrates under high- NO_x conditions. Consequently the formation of SOA from certain biogenic hydrocarbons such as sesquiterpenes may be more efficient in polluted air.

7.2 Introduction

Atmospheric oxidation of certain volatile organic compounds (VOCs) leads to the formation of low volatility species that partition into the condensed phase and form secondary organic aerosol (SOA). Biogenic hydrocarbons, such as isoprene (C_5H_8), monoterpenes ($\text{C}_{10}\text{H}_{16}$), and sesquiterpenes ($\text{C}_{15}\text{H}_{24}$), are important contributors to the

total atmospheric burden of SOA owing to their large global emissions and high reactivity with hydroxyl radicals (OH), ozone (O₃), and nitrate radicals (NO₃) (Guenther et al., 1995; Griffin et al., 1999a; Geron et al., 2000; Owen et al., 2001; Atkinson and Arey, 2003; Seinfeld and Pankow, 2003; Kanakidou et al., 2005).

Over the last two decades, numerous laboratory chamber experiments have been conducted to study aerosol formation from biogenic hydrocarbons. The NO_x level has been found to be highly influential in SOA production for a variety of compounds. Recent studies on isoprene photooxidation, α -pinene ozonolysis, limonene ozonolysis, and benzene, toluene, and *m*-xylene photooxidation have demonstrated that a larger aerosol yield is observed under low-NO_x conditions (Kroll et al., 2005, 2006; Presto et al., 2005; Zhang et al., 2006; Ng et al., 2007). Competitive chemistry of peroxy radicals between NO and HO₂, with the HO₂ reaction route producing products of lower volatility, seems consistent with these observations (Hatakeyama et al., 1991; Johnson et al., 2004, 2005; Kroll et al., 2005, 2006; Presto et al., 2005; Ng et al., 2007). For example, in α -pinene ozonolysis Presto et al. (2005) observed relatively volatile organic nitrates under high-NO_x conditions, while less volatile products, such as 10-hydroxypinonic acid, were more abundant under low-NO_x conditions. Although the increase in SOA yield at low-NO_x conditions has now been well-established for isoprene, α -pinene, limonene, and benzene, toluene, and *m*-xylene, a key question is – do larger molecules, especially the sesquiterpenes, exhibit a similar NO_x-dependence of SOA yield?

In the present study, we focus on two sesquiterpenes, longifolene and aromadendrene, and compare the NO_x-dependence of their SOA formation with that of

α -pinene. Longifolene reacts very slowly with ozone (Atkinson and Arey, 2003), making it ideal for study of OH photooxidation. Moreover, both longifolene and aromadendrene have only a single double bond; one can infer more easily the general oxidation mechanisms in SOA formation than when multiple double bonds are present (Ng et al., 2006). Experiments are conducted under limiting NO_x conditions (high- NO_x conditions in which HONO is used as the OH precursor, and low- NO_x conditions in which H_2O_2 is used as the OH precursor), as well as by systematically varying the level of NO_x , using well-established protocols for studying SOA formation.

7.3 Experimental Section

Experiments are performed in Caltech's dual 28 m³ Teflon environmental chambers. Details of the facilities have been given elsewhere (Cocker et al., 2001; Keywood et al., 2004). Before each experiment, the chambers are flushed continuously with dry purified air for ~24 h. Each chamber has a dedicated Differential Mobility Analyzer (DMA, TSI model 3081) coupled with a condensation nucleus counter (TSI model 3760) for measuring aerosol size distribution, number concentration, and volume concentration. All aerosol growth data are corrected for wall loss, in which size-dependent coefficients determined from inert particle wall loss experiments are applied to the aerosol volume data (Keywood et al., 2004). Temperature, relative humidity (RH), O_3 , NO, and NO_x are continuously monitored. The initial temperature of the chamber is ~20°C. Heating from the lights leads to a temperature increase of approximately 5°C inside the chamber over the course of the experiment. The analytical instruments are located outside the chamber enclosure and are at the temperature of the surrounding room (~20-22°C). The air may cool slightly as it is sampled from the chamber into the

instruments, and the measured aerosol likely corresponds to the gas-particle partitioning at the temperature of the surrounding room rather than the chamber enclosure. Such small temperature difference is unlikely to affect the results significantly.

Seed particles are introduced into the chamber to act as a substrate onto which the gas-phase semivolatile products may condense. Seed aerosols are generated from a 0.015M aqueous ammonium sulfate solution with a constant-rate atomizer, producing initial particle number concentrations of about 25,000 particles cm^{-3} , with a geometric mean diameter of about 50 nm, and initial aerosol seed volume of $\sim 10\text{-}15 \mu\text{m}^3 \text{cm}^{-3}$. After introduction of the seed aerosol, a known volume of the parent hydrocarbon is injected into a glass bulb, and then introduced into the chambers by an air stream. For experiments with α -pinene and longifolene, the concentration (mixing ratio) of the parent hydrocarbon is monitored with a Hewlett Packard gas chromatograph (model 5890) with flame ionization detection (GC-FID). Owing to the difficulties in measuring aromadendrene with GC-FID, its concentration is measured with a Proton Transfer Reaction Mass Spectrometer (PTR-MS), a custom-modified Varian 1200 system (see the Appendix). Under typical chamber conditions aromadendrene concentrations are measured with an uncertainty of about $\pm 22\%$.

In the high- NO_x experiments nitrous acid (HONO) serves as the OH precursor. It is introduced into the chamber after injection of the seed aerosol and parent hydrocarbon. HONO is prepared by dropwise addition of 15 mL of 1% NaNO_2 into 30 mL of 10% H_2SO_4 in a glass bulb. The bulb is then attached to the chamber and a stream of dry air is passed through the bulb into the chamber. NO and NO_2 , formed as side products in the preparation of HONO, are also introduced into the chamber, and are measured by a

commercial NO_x monitor (Horiba APNA-360, Irvine, CA). Additional NO from a 500 ppm gas cylinder (Scott Marrin, Inc.) is introduced into the chamber after the addition of HONO to achieve a target NO_x level in the chamber of about 1 ppm (upper detection limit of the NO_x monitor).

For low-NO_x experiments, H₂O₂ serves as the OH precursor. The background NO_x level in the chamber during such experiment is ≤ 2 ppb. About 3 ppm H₂O₂ is introduced into the chamber (prior to introduction of seed particles and parent hydrocarbon) by bubbling air through a 50% H₂O₂ solution for 2.5 h at 5 L/min. The air stream then passes through a particle filter to remove any droplets. Variable NO experiments are also carried out, in which a known quantity of NO is introduced into the chamber after the addition of H₂O₂.

Once the seed, parent hydrocarbon, and NO_x concentrations stabilize, reaction is initiated by irradiating the chamber with blacklights. Output from the lights is between 300 and 400 nm, with a maximum at 354 nm. Half of the available black lights are used in the experiments. At these wavelengths HONO efficiently photolyzes to OH and NO. By contrast, H₂O₂ absorbs only weakly in this wavelength range, requiring the use of ppm mixing ratios of H₂O₂ to achieve target levels of OH.

A comprehensive range of measurements are employed to study the chemical composition of the SOA formed. Real-time particle mass spectra are obtained with an Aerodyne quadrupole Aerosol Mass Spectrometer (Q-AMS) (Jayne et al., 2000; Bahreini et al., 2005). A Particle-Into-Liquid Sampler (PILS, Brechtel Manufacturing, Inc.) is employed for quantitative measurements of water-soluble ions in the aerosol phase (Sorooshian et al., 2006). For offline chemical analysis, Teflon filters (PALL Life

Sciences, 47-mm diameter, 1.0- μm pore size, teflo membrane) are collected at the point when aerosol volume reaches its maximum value. Depending on the total chamber volume concentration of aerosol, the filter sampling time is 2-4 h, which results in $\sim 1.5\text{-}6\text{ m}^3$ of total chamber air sampled. Teflon filter extraction protocols in HPLC-grade methanol have been described previously (Surratt et al., 2006). The resultant filter extracts are then analyzed by the following suite of analytical techniques: high performance liquid chromatography/electrospray ionization-quadrupole mass spectrometry (HPLC/ESI-MS), electrospray ionization-ion trap mass spectrometry (ESI-ITMS), and matrix-assisted laser desorption ionization-time-of-flight mass spectrometry (MALDI-TOFMS); details of the protocols are described elsewhere (Surratt et al., 2006).

In addition to the above analytical techniques, filter extracts (in 1:1 (v/v) solvent mixture of methanol and 0.1% aqueous acetic acid solution) are also analyzed by a Waters ACQUITY ultra performance liquid chromatography (UPLC) system, coupled with a Waters LCT Premier time-of-flight (TOF) mass spectrometer (MS) equipped with an electrospray ionization (ESI) source. The ESI source on this instrument contains two individual sprays; one spray is for the eluent and the other is for the lock-mass correction. Optimum ESI conditions are found using a 2.5 kV capillary voltage, 40 V sample cone voltage, 350°C desolvation temperature, 130°C source temperature, 20 L hr⁻¹ cone gas flow rate, and a 650 L hr⁻¹ desolvation gas flow rate. Data are collected from m/z 50-1000 in the negative (-) ionization mode using the TOFMS operated in the W geometry reflectron mode. The W reflectron mode offers the highest mass resolution, which is approximately 12000, and allows for exact mass measurements to be conducted on detected SOA components. The chromatographic separations are carried out on a Waters

ACQUITY HPLC HSS (high strength Silica) column (2.1 x 100 mm, 1.8 μm particle size) at 45°C using a gradient elution scheme. The eluent composition is (A) 0.1% acetic acid in water and (B) 0.1% acetic acid in methanol; both eluents are high purity solvents (LC-MS ChromaSolv Grade, Sigma-Aldrich). In the 12-min gradient elution program used, the concentration of eluent B is 0% for the first 2 min, increased to 90% from 2 to 10 min, held at 90% from 10 to 10.2 min; and then decreased back to 0% from 10.2 to 12 min. The flow rate of the eluent is 0.3 mL min⁻¹ and the sample injection volume is 2 μL . At the beginning of each analysis period, the TOFMS is calibrated using a 1:1 (v/v) solvent mixture of acetonitrile and 0.1% phosphoric acid aqueous solution. During each chromatographic run, 2 ng/ μL of leucine enkephalin (MW = 555) is used for the lock-mass spray for lock-mass correction to obtain accurate masses for each SOA component eluting from the column. The lock-mass syringe pump is operated at 20 $\mu\text{L min}^{-1}$. In addition to the lock-mass spray, the dynamic range enhancement feature of this mass spectrometer is applied to prevent dead time, which affects mass accuracy, from occurring. As confirmation of the UPLC/ESI-TOFMS technique, a standard sample containing known isoprene and α -pinene sulfate esters previously characterized by Surratt et al. (2007) are analyzed. The known elemental compositions (i.e. molecular formulas) of the previously characterized sulfate esters (Surratt et al., 2007) are in excellent agreement with their measured exact masses (i.e. within ± 2 mDa or ± 2 ppm). In addition to exact mass measurements, further insights into the structures of the SOA components is obtained by generating tandem MS data, which are generated by increasing the first aperture voltage on the TOFMS from 10 V to 25 V.

The parent aromatics studied (shown in Table 7.1) and their stated purities are as follows: α -pinene (Aldrich, 99+%), longifolene (Aldrich, >99%), and aromadendrene (Aldrich, >97%). Experimental conditions and results for each of the parent hydrocarbons studied are given in Tables 7.2, 7.3, and 7.4. In calculating SOA yield, knowledge of the SOA density is required. By comparing volume distributions from the DMA and mass distributions from the Q-AMS, effective densities for the SOA formed can be estimated (Bahreini et al., 2005, Alfarra et al., 2006). The estimated densities of the SOA formed from different parent hydrocarbons are given in Table 7.5.

7.4 Aerosol Yields

7.4.1 α -pinene photooxidation

Under high-NO_x conditions, the efficient photolysis of HONO generates relatively high concentrations of OH ($\sim 2 \times 10^7$ molecules cm⁻³ initially), leading to rapid α -pinene decay. Aerosol growth occurs essentially immediately even when [NO] is high (100's of ppb). With the high NO concentration throughout the entire experiment, formation of ozone (and also NO₃) is suppressed.

Under low-NO_x conditions, aerosol growth is also observed immediately after initiation of irradiation. The α -pinene decays at a slower rate than under high-NO_x conditions, owing to the relatively slow production of OH radicals by H₂O₂ photolysis. Ozone formation is observed at an increasing concentration over time (~ 30 ppb at the peak of aerosol growth). Based on the reaction rate constants of α -pinene + O₃ (k_{ozone}) and α -pinene + OH (k_{OH}), and an inferred OH concentration of 3×10^6 molecules cm⁻³, it is estimated that an ozone source of ~ 0.1 ppb/min would be required to produce the

observed α -pinene decay. It is estimated that only about 35% of the α -pinene reacts by ozonolysis at the point of maximum growth. Therefore, while α -pinene ozonolysis accounts for some of the SOA yield under low- NO_x conditions, it is highly unlikely that the observed yield difference between high- and low- NO_x arises solely from the presence of ozone.

Figure 1 shows the time-dependent growth curves (organic aerosol generated, denoted as ΔM_o , as a function of hydrocarbon reacted ΔHC) for α -pinene under different NO_x conditions. As hydrocarbon measurements are made with a lower frequency than those of particle volume, the α -pinene concentrations shown are obtained by interpolating the GC measurements. In all cases, the initial mixing ratio of α -pinene was about 15 ppb, all of which was consumed by the end of the experiment. It is clear that the aerosol growth under low- NO_x (H_2O_2) conditions substantially exceeds that under high- NO_x (HONO) conditions, while the intermediate NO_x (" $\text{H}_2\text{O}_2 + \text{NO}$ ") experiment exhibits an aerosol yield between those of the two extremes. The time-dependent growth curve of the " $\text{H}_2\text{O}_2 + \text{NO}$ " experiment exhibits a vertical section at the end, indicating that further reactions are contributing to aerosol growth after the α -pinene is consumed. We return to this observation in Section 7.6.2.2.

7.4.2 Longifolene photooxidation

For longifolene, a series of high- NO_x (HONO) experiments and low- NO_x (H_2O_2) experiments with varying initial hydrocarbon concentrations were carried out. The time-dependent growth curves for 3 high- NO_x and 3 low- NO_x experiments, with initial longifolene mixing ratios ranging from ~ 10 to 30 ppb, are shown in Fig. 2. In contrast to α -pinene photooxidation, longifolene aerosol yields under high- NO_x conditions exceed

those under low-NO_x conditions. Under high-NO_x conditions, the maximum SOA yield (about ~100-130%; note that yield is defined on a mass basis) is reached in ~10 min after initiation of the experiments, with the yield decreasing after that point. Under low-NO_x conditions, SOA yield continues to increase over the course of the experiment, reaching a maximum when all the longifolene is consumed. The final SOA yields of each longifolene low-NO_x experiment actually lie on a straight line that passes through the origin, indicating that under low-NO_x conditions SOA yield is constant, at ~75%. Based on the observed longifolene decay and k_{OH} for longifolene, the chamber OH concentration under low-NO_x conditions is estimated to be $\sim 3 \times 10^6$ molecules cm⁻³.

The effect of NO_x on longifolene aerosol formation is further illustrated by the time-dependent growth curves in Fig. 3. In both experiments H₂O₂ is used as the OH precursor and the initial longifolene mixing ratio is ~4.3 ppb, with only the amount of NO differing; in one experiment no extra NO is added, while in the other experiment about 300 ppb of NO is introduced into the chamber after the addition of H₂O₂. Aerosol growth in the presence of ~300 ppb NO is substantially higher. A series of experiments with the same initial longifolene concentration but different initial NO concentrations (~100-600 ppb) are also carried out. Figure 4 shows the final aerosol yield as a function of the initial NO_x concentration. The amount of aerosol formed is highly dependent on the level of NO_x present initially; with ~600 ppb NO, the ultimate aerosol yield is twice that at low-NO_x conditions.

7.4.3 Aromadendrene photooxidation

Figure 5 shows the final aerosol yield as a function of initial NO_x concentration for aromadendrene photooxidation. The OH precursor used in these experiments is H₂O₂

and the initial aromadendrene mixing ratio is ~ 5 ppb. In these experiments the concentration of aromadendrene is monitored with the PTR-MS with an uncertainty of about $\pm 22\%$. Despite uncertainties in the aromadendrene measurements, it is clear that aromadendrene aerosol yield increases with NO_x concentration; similarly to longifolene, with ~ 500 ppb NO, the aerosol yield is doubled over that at low- NO_x conditions.

7.5 Chemical composition of SOA

In this section, the chemical composition of α -pinene and longifolene SOA are presented. The aromadendrene experiments are performed mainly to verify the observed NO_x dependence for longifolene, in which SOA yield is higher under high- NO_x conditions. Thus, detailed analysis of the chemical composition of aromadendrene SOA is not pursued.

7.5.1 Aerosol Mass Spectrometer (Q-AMS) measurements

Figures 6 and 7 show the AMS high- NO_x versus low- NO_x spectrum signal for α -pinene and longifolene photooxidation, respectively. Each mass fragment is normalized by the total signal. All spectra have prominent signals at m/z 43 (CH_3CO^+) and m/z 44 (CO_2^+), indicating that the aerosols are highly oxidized and are dominated by carbonyl-containing compounds and multifunctional carboxylic acids. Mass fragment 29 can arise from C_2H_5^+ or CHO^+ , and mass fragment 41 can arise from C_3H_5^+ or C_2HO^+ ; given the highly oxidized nature of the aerosols, they are more likely to be the latter. Though the above mass fragments are prominent in all spectra, the relative contribution of each m/z is different for low- and high- NO_x spectra for both α -pinene and longifolene, suggesting that aerosol compositions are different under different NO_x conditions. The common

feature in the α -pinene and longifolene spectra is that there is a significant contribution from m/z 30 and m/z 46 under high-NO_x conditions for both compounds.

The contribution of m/z 30 and m/z 46 to the total organic mass under different NO_x conditions can be examined more directly by examining $[m/z$ 30 + m/z 46]/[Organic mass] as a function of the total organic mass. As seen in Figs. 8 and 9, for both α -pinene and longifolene, respectively, this ratio is very small under low-NO_x conditions (~2%) and ~15-25% under high-NO_x conditions. The m/z 30 (NO⁺) and m/z 46 (NO₂⁺) signals are commonly associated with nitrate species; the significance of these mass fragments will be discussed further in Section 7.6.1.

Changes in AMS spectra over the course of the experiment for longifolene under high- and low-NO_x conditions are shown in Figs. 10 and 11, respectively, for which the corresponding growth curves appears in Fig. 2 (the pair of experiments with ~30 ppb of longifolene injected). In Figs. 10 and 11, the top panel shows the fractional contribution of each mass fragment to the total organic and nitrate signal during the growth phase of the experiment (Δ H_C~100 μ g m⁻³ in Fig. 2); the bottom panel shows the percentage change of each mass fragment from the growth phase to the point at which all of the hydrocarbon is consumed (Δ H_C~200 μ g m⁻³ in Fig. 2). Under high-NO_x conditions, changes in mass fractions of different fragments during aerosol growth are minimal, indicating that the aerosol composition is not changing significantly over time. Under low-NO_x conditions, however, the mass fraction of m/z 44 increases by 93% as the oxidation progresses, while those for higher m/z 's are observed to decrease. The mass fractions of m/z 44 and higher m/z 's continue to change even after the aerosol growth

levels off, suggesting the presence of further chemistry (either gas-phase or particle-phase) even after all the initial hydrocarbon is consumed.

7.5.2 Offline chemical analysis

All of the ions detected by the UPLC/ESI-TOFMS instrument from α -pinene and longifolene photooxidation under different NO_x conditions are listed in Tables 7.6 and 7.7, respectively. The tables list the exact masses and their likely molecular formulas that corresponding to each of the $[\text{M} - \text{H}]^-$ ions detected, where M is the molecular weight of the compound. The error between the measured mass and theoretical mass is reported in two different ways, ppm and mDa. For most of the ions observed, the error between the measured and theoretical masses is less than ± 2 mDa and ± 5 ppm, which is considered as excellent resolution for small molecules (i.e. compounds less than 1000 Da). Solvent blanks and control filters were also run on the UPLC/ESI-TOFMS instrument; none of the listed ions is observed in either of these control samples, indicating that these ions are not contaminant ions introduced during sample workup. The ions listed in Tables 7.6 and 7.7 are also detected by HPLC/ESI-MS and ESI-ITMS, confirming that these compounds are not the result of artifact formation in a specific mass spectrometer.

Acidic compounds, such as carboxylic acids and sulfate esters, readily ionize under (-)ESI-MS techniques (Gao et al., 2004; Surratt et al., 2006; Surratt et al., 2007). Hydroxylated compounds, as well as ketones and aldehydes, however, are not ionizable unless carboxylic acid and/or sulfate ester moieties are also present within the same molecule. Therefore, it is expected that the UPLC/ESI-TOFMS data are sensitive only to acidic compounds. For the SOA formed in the presence of NO_x , (HONO and “ $\text{H}_2\text{O}_2 + \text{NO}$ ” experiments), even $[\text{M} - \text{H}]^-$ ions are observed in ESI mass spectra, indicating the

compound has an odd number of organic nitrate functional groups, as previously observed in isoprene SOA formed under high-NO_x conditions (both HONO and ‘H₂O₂ + NO’) (Surratt et al. 2006). For α-pinene, only one acidic organic nitrate (*m/z* 322) is detected in the HONO experiment and none is detected in H₂O₂ and intermediate NO_x experiments. Most of these ions detected in the α-pinene experiments have been identified in previous laboratory work (Glasius et al., 1999; Glasius et al., 2000; Larsen et al., 2001) and field studies (Gao et al., 2006). For longifolene, a much wider array of acidic organic nitrates is detected by the UPLC/ESI-TOFMS instrument in both HONO and ‘H₂O₂ + NO’ experiments.

Figure 12 shows the extracted ion chromatograms (EICs) of *m/z* 346, 374, and 390 from longifolene oxidation under different NO_x conditions. These *m/z* values correspond to acidic organic nitrates, as confirmed by the exact mass data (Table 7.7) and by their even [M – H][–] ions. The chromatographic peaks are much larger in the highest NO_x experiment than those in the ‘H₂O₂ + NO’ experiment (except *m/z* 372); no chromatographic peaks are observed under low-NO_x (H₂O₂) conditions. Besides the detection of more organic nitrates in the highest NO_x experiment, for several [M – H][–] ions (e.g. *m/z* 374 and 390) there are more structural isomers present. When comparing the chromatographic peaks for the non-organic nitrate species (e.g. *m/z* 223, 239, 253, 255, 267, 269, and 283), it is found that these peaks are larger under low-NO_x conditions, indicating differing SOA composition in the absence of NO_x.

7.6 Discussion

7.6.1 Effect of hydrocarbon size on NO_x dependence

It has been established that NO_x levels exert a major influence on SOA formation (Hatakeyama et al., 1991; Pandis et al., 1991; Zhang et al., 1992; Hurley et al., 2001; Johnson et al., 2004, 2005; Song et al., 2005; Presto et al., 2005; Kroll et al., 2005, 2006; Zhang et al., 2006; Ng et al., 2007). For photooxidation of isoprene, SOA yields increase as the NO_x level decreases (Kroll et al., 2006). The proposed mechanism for this observed NO_x dependence is the competitive chemistry of organic peroxy radicals between NO and HO₂, in which the semivolatile products formed via the RO₂ + HO₂ path are less volatile than those formed via the RO₂ + NO route (Hatakeyama et al., 1991; Johnson et al., 2004, 2005; Presto et al., 2005; Kroll et al., 2006; Zhang et al., 2006; Ng et al., 2007). A similar yield dependence on NO_x is observed here for photooxidation of α -pinene as for isoprene (Fig. 1). For an initial α -pinene concentration of \sim 15 ppb, the SOA yield under low-NO_x conditions is about a factor of 3 higher than that under high-NO_x conditions. The observed NO_x dependence is consistent with that of previous studies on α -pinene photooxidation (Hatakeyama et al., 1991; Zhang et al., 1992).

The observed NO_x dependence of SOA yield for the sesquiterpenes is, however, different from that of isoprene and α -pinene. For longifolene and aromadendrene, aerosol yield increases with increasing NO_x concentration (Figs. 2-5). This reversal of the NO_x dependence of SOA formation could be the result of a number of factors. Figure 13 shows a simplified reaction mechanism involving peroxy radical chemistry. At the two limiting NO_x conditions of this study, the peroxy radical chemistry is relatively well-defined; under high-NO_x conditions, peroxy radicals react virtually entirely with NO,

while under low-NO_x conditions, RO₂ reacts predominantly with HO₂. One of the possible explanations for the higher SOA yield under high-NO_x conditions is the formation of large alkoxy radicals that isomerize rather than fragment. Isomerization is plausible if the alkoxy radical has four or more carbon atoms and can form a 6-membered transition state (Baldwin et al., 1977; Carter and Atkinson, 1985). The isomerization pathway leads to the formation of larger, multifunctional products that are likely less volatile. The relative importance of isomerization increases with the size of alkoxy radicals (Atkinson, 1994, 1997a, 1997b; Atkinson et al., 1995; Atkinson et al., 1999), and larger compounds could exhibit increasing SOA yields under high-NO_x conditions as a consequence of this mechanism. For example, Lim et al. (2005) measured SOA yields up to ~50% for C₁₅ alkanes in the presence of ppm levels of NO_x. In their study, multiple isomerization steps have been proposed to lead to the formation of multifunctional compounds including nitrooxy, hydroxyl, and carbonyl groups, and it is suggested that the hydroxycarbonyls formed isomerize to form furan species that can undergo further reaction (Lim et al., 2005). Gas-phase products that are consistent with the isomerization mechanism have been observed in α -pinene photooxidation but this pathway does not appear to dominant SOA formation under high-NO_x conditions (Aschmann et al., 1998, 2002). Such a mechanism is consistent with the observed NO_x dependence of SOA yield for longifolene and aromadendrene.

Higher sesquiterpene SOA yields observed under high-NO_x conditions may, secondly, be a result of the formation of relatively nonvolatile organic nitrates, evidence for which appears in both Q-AMS data and filter sample data. As shown in Figs. 8 and 9, for both α -pinene and longifolene, the ratio of the sum of m/z 30 (NO⁺) and m/z 46

(NO₂⁺) to the total organic mass is higher under high-NO_x conditions. The ratio $[m/z\ 46]/[\text{Organic mass}]$ follows the same trend as that of $[m/z\ 30 + m/z\ 46]/[\text{Organic mass}]$ as a function of organic mass, indicating that $m/z\ 30$ and $m/z\ 46$ are correlated. It is possible that the signal at $m/z\ 30$ could be the result of a non-nitrogen containing organic fragment ion; however, given the observed correlation between $m/z\ 30$ and $m/z\ 46$, the unlikely case of an organic fragment ion at $m/z\ 46$, and the small signals under low-NO_x conditions, it appears that there is little interference from organics at these signals and their presence is indicative of nitrate formation. Under high-NO_x conditions, PILS/IC analysis, which measures only inorganic ions, shows that $\sim 10\ \mu\text{g m}^{-3}$ of nitrates are present in the aerosol. These inorganic nitrates may arise from the partitioning of gas-phase HNO₃ into the aerosol phase, and they will contribute to some of the AMS signals at $m/z\ 30$ and 46 . Assuming no non-nitrate contribution to $m/z\ 30$ and 46 , the total nitrate content of the SOA is estimated as the sum of the signals at each fragment. It is found that the calculated nitrate content exceeds that measured by PILS/IC, suggesting the presence of organic nitrates. It is emphasized that $m/z\ 30$ and $m/z\ 46$ are used only as a qualitative indication of the presence of organic nitrates.

The filter sample data provide a more direct comparison on the amount of organic nitrates formed in α -pinene and longifolene photooxidation under different NO_x conditions. For both α -pinene and longifolene, no acidic nitrates are observed under low-NO_x conditions, consistent with the prevalent RO₂ + HO₂ reaction in this case. Organic nitrate yield from the RO₂ + NO reaction increases with increasing carbon number (Atkinson et al., 1987; Carter and Atkinson, 1989; O'Brien et al., 1998; Arey et al., 2001; Aschmann et al., 2001; Zhang et al., 2004), and with the larger carbon chain the organic

nitrates formed are likely to be less volatile, an observation that is consistent with the much wider array and larger quantities of acidic nitrates detected in longifolene photooxidation under high-NO_x conditions. Hence for photooxidation of larger compounds such as sesquiterpenes, the nitrate formation channel may play an important role in SOA formation under high-NO_x conditions. With the addition of atoms such as O and N, mass-based SOA yields from longifolene photooxidation under high-NO_x conditions actually exceed 100%. Tandem MS data (generated by increasing the aperture voltage from 10 to 25 V on the UPLC/ESI-TOFMS instrument) for the C₁₇ acidic organic nitrates (i.e. *m/z* 342, 374, and 390) from longifolene photooxidation reveal a common neutral loss of 60 Da, which possibly corresponds to an acetic acid monomer. Surratt et al. (2006) and Szmigielski et al. (2007) have recently shown that particle-phase esterification occurs in isoprene SOA formed under high-NO_x conditions; specifically a 2-methylglyceric acid monomer (known isoprene ambient SOA tracer compound) can react with an acetic acid monomer to create a 2-methylglyceric acid dimer mono-acetate derivative. The observed neutral loss of 60 Da for these C₁₇ acidic organic nitrates suggests that these compounds may be dimers formed by particle-phase esterification.

Lacking appropriate analytical techniques for the detection of non-acidic nitrates, the contribution of these species under high-NO_x conditions cannot be assessed. In α -pinene photooxidation, hydroxynitrates have been identified in the gas phase using mass spectrometry (Aschmann et al., 1998, 2002). In SOA formation from alkanes under high-NO_x conditions, Lim et al. (2005) found that, while SOA from oxidation of C₁₀ alkane contains no δ -hydroxynitrates, such compounds contribute ~40% of the SOA mass for

reactions of the C₁₅ alkane. It is likely that a larger quantity of hydroxynitrates are present also in the longifolene system, as compared to α -pinene.

7.6.2 General mechanisms of aerosol growth

7.6.2.1 Loss of semivolatiles

Substantial insights into the general mechanism of SOA formation and growth kinetics can be gained by examining so-called growth curves (Ng et al., 2006, 2007). Figure 2 shows the time-dependent growth curves from longifolene photooxidation under high- and low-NO_x conditions. The high-NO_x growth curves have a “convex” shape, indicating that aerosol growth slows down as longifolene approaches complete reaction. Similar behavior for longifolene growth was observed by Ng et al. (2006), who suggested that this atypical growth behavior may have been spurious, as a result of inaccuracies in PTR-MS measurements, owing to interference from products, or fragments of products with the same mass to charge ratio as longifolene; or a change in the aerosol density over the course of the experiment. In this study, in those experiments in which the longifolene concentration was monitored by both GC-FID and PTR-MS, the shape of PTR-MS hydrocarbon decay agrees with that measured by GC-FID. The density of the aerosol is estimated during oxidation by comparing Q-AMS and DMA data. It is found that the SOA density decreases slightly (<5%) over the course of the experiment, however, such a small decrease in density is within experimental uncertainty and cannot account for the observed atypical growth behavior.

Deceleration in SOA growth can arise from the loss of semivolatiles by photolysis, further reaction with OH to form volatile products, or deposition loss to

chamber walls. When fitting the observed aerosol growth with a simple kinetic system that accounts for gas-phase loss of semivolatile oxidation products (Fig. 14), it is estimated that the first-order gas-phase loss rate constant (k_g) is about 5 times larger than the pseudo-first-order oxidation rate of the parent hydrocarbon ($k'_{OH} = k_{OH}[OH]$). At the estimated OH concentration of $\sim 2 \times 10^7$ molecules cm^{-3} under high- NO_x conditions, k'_{OH} for longifolene is $\sim 9.6 \times 10^{-4} \text{ s}^{-1}$. Under high- NO_x conditions, the loss of organic nitrates (among other gas-phase species) may play a role in the observed deceleration in aerosol growth. The reaction rate constants of small alkyl nitrates with OH are generally of the order of $10^{-13} \text{ cm}^3 \text{ molecule}^{-1} \text{ s}^{-1}$ (hence pseudo-first-order reaction rate of $\sim 10^{-6} \text{ s}^{-1}$) and their photolysis rates have been measured to be $\sim 1 \times 10^{-6} \text{ s}^{-1}$ (Talukdar et al., 1997; Finlayson-Pitts and Pitts, 2000). Although the OH reaction rate and photolysis rate of organic nitrates are much slower than the oxidation rate of longifolene, both rates are expected to increase with carbon number (Talukdar et al., 1997; Finlayson-Pitts and Pitts, 2000; Treves et al., 2003). Hence, it is possible that gas-phase reaction of C_{15} organic nitrates may be occurring at an appreciable rate. From the change in AMS spectra from longifolene photooxidation under high- NO_x conditions (Fig. 10), it is found that both m/z 30 and 46 decrease by $\sim 10\%$ over the course of the photooxidation. Further study on the OH reaction rate constant and photolysis rate of larger nitrates would be useful in evaluating the importance of gas-phase nitrate chemistry in aerosol formation.

As a possible explanation of decreasing SOA volume during the photooxidation of isoprene under low- NO_x conditions, Kroll et al. (2006) suggest photolysis of organic hydroperoxides in the gas phase, and/or particle-phase photolysis, or further reactions of OH radicals to form products of higher volatility that partition back to the gas phase may

be occurring. From the AMS data on the percentage change in the mass fraction of different mass fragments under low-NO_x conditions (Fig. 11), it is found that m/z 44 increases over the course of the oxidation while other higher m/z values decrease. The signal at m/z 44 (CO₂⁺) is often used as a tracer for oxidized aerosol (Zhang et al., 2005); thus, an increase in m/z 44 may be indicative of further oxidization of SOA. In comparison to the dramatic decrease in SOA volume observed in isoprene photooxidation, the compounds formed from further oxidations of longifolene products are still sufficiently nonvolatile that they do not repartition back into the gas phase. Also the photolysis and the OH reaction rate constants for larger hydroperoxides may not be as rapid as those formed in the isoprene system. While no gas-phase data regarding the photolysis and OH reaction rate for larger organic peroxides are available, a recent study on the photooxidation of methyhydroperoxide and ethylhydroperoxide in the aqueous phase indicates that the photolysis and OH reaction rates for the latter are indeed slower than those of methyhydroperoxide (Monod et al., 2007). The photochemistry of larger and more complex hydroperoxides merits further investigation.

7.6.2.2 SOA formation from higher generation products

In Figs. 1 and 3, the growth curves of α -pinene and longifolene photooxidation exhibit a “hook” at the end of the intermediate NO_x experiments, indicating that aerosol growth continues after the complete consumption of the parent hydrocarbon. Organic mass measured by the Q-AMS increases even after all the hydrocarbon is consumed, indicating that this additional aerosol growth is not a result of condensation of inorganic nitrate. Continued aerosol growth can arise from further gas-phase reactions of reactive oxidation products, such as aldehydes and furans, etc, or from further particle-phase

reactions. In the intermediate NO_x experiments, the NO concentration goes to zero about 30 min after the commencement of photooxidation, owing to the rapid reaction of NO and peroxy radicals (HO_2 and other peroxy radicals). As a result, a transition from high- NO_x to low- NO_x conditions occurs over the course of the experiment, and the final aerosol formed is potentially a mixture of the products formed under both conditions. Johnson et al. (2004, 2005) proposed the formation of peroxyhemiacetals from hydroperoxides and aldehyde species as an effective mechanism for the higher aerosol yield observed from photooxidation of aromatics under low- NO_x conditions. Such type of particle-phase reactions may be contributing to the further aerosol growth observed in the intermediate NO_x experiments.

7.7 Implications

A series of chamber experiments investigating the NO_x dependence of SOA formation from the photooxidation of one monoterpene and two sesquiterpenes is reported here. Monoterpene SOA formation, such as from α -pinene, is found to follow the same NO_x dependence as isoprene, in which the aerosol yields are substantially higher under low- NO_x conditions. The NO_x dependence of SOA formation from the two sesquiterpenes is, however, markedly different from those of isoprene and α -pinene; for longifolene and aromadendrene, aerosol yields are at their maximum under high- NO_x conditions. The reason for this reversal of the NO_x dependence of SOA formation for the sesquiterpenes, while not unequivocally established here, may be the result of production of highly nonvolatile organic nitrates, the existence of which is suggested by both Q-AMS and filter sample data. Since larger alkoxy radicals can isomerize more readily, the

higher SOA yields observed under high-NO_x conditions suggests also that isomerization may be an effective channel for SOA production for larger hydrocarbon precursors.

The increase in SOA yield from photooxidation of the larger biogenic hydrocarbons under high-NO_x conditions could have implications in terms of the effect of anthropogenically influenced air masses on biogenic SOA formation. In the recent study of de Gouw et al. (2005), it is suggested that over the western Atlantic the majority of the measured organic aerosol is from secondary anthropogenic sources, a conclusion that is not consistent with the radiocarbon measurements that indicate high fractions of “modern”, biogenic carbon (e. g. Klinedinst and Currie, 1999). If the production of SOA from biogenic hydrocarbons is enhanced in the presence of NO_x, observations of enhanced SOA correlated with anthropogenic sources can occur, even for organic carbon of biogenic origin. Large anthropogenic hydrocarbons may exhibit a similar NO_x behavior as that of the sesquiterpenes studied, as suggested by the substantial SOA yields from the OH-initiated reaction of large alkanes in the presence of ppm levels of NO_x (Lim et al., 2005). If the NO_x behavior observed for longifolene and aromadendrene extends to other sesquiterpenes as well as larger alkanes, the contribution to the total SOA from these compounds in polluted air may actually be higher than already estimated (Griffin et al., 1999ab; Carreras-Sospedra et al., 2005; de Gouw et al. 2005).

In this study, we have investigated only the NO_x dependence of SOA formation from photooxidation of the monoterpene α -pinene and two sesquiterpenes, each containing only one double bond. SOA formation from compounds with two or more double bonds can exhibit characteristics that suggest significant contributions from multiple generation products (Ng et al., 2006) and this may have impacts on the NO_x

dependence. It is clear that the effect of NO_x on SOA yields from the complete suite of ambient aerosol-forming hydrocarbons should be evaluated thoroughly.

7.8 Appendix: Description of PTR-MS technique

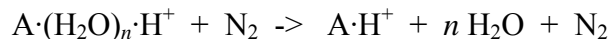
For PTR-MS sampling, a constant flow of ~ 2.5 standard liters per minute (slm) is drawn from the chamber through PFA tubing. The residence time in the inlet tubing is roughly 1 s. A small portion of the flow, 93 standard cubic centimeters per minute [sccm], is pulled through a glass critical orifice into a 2.54-cm diameter glass flow tube, in which this sample flow is diluted with dry N_2 (1.6 slm) to maintain the flow tube pressure at 35 mbar. This dilution minimizes confounding effects owing to large concentrations of hydrogen peroxide and other compounds typically used or produced in chamber experiments.

In the flow tube, analyte ionization occurs in a manner similar to that described by Crouse et al. (2006) for negative ionization. N_2 (400 sccm) flows through an ion source cup composed of a cylindrical silver foil lined with ^{210}Po and sealed with gold. α bombardment from the ^{210}Po , coupled with trace water present in the N_2 , leads to the formation of positively charged clusters, e.g., $(\text{H}_2\text{O})_n\text{H}^+$. The electric potentials of the ion source components are set such that these positively charged clusters then pass through a 6.35 mm aperture into the 35 mbar flow tube, flowing perpendicular to the sample flow. The clusters then react via proton transfer with the analyte, in the present case aromadendrene, in the sample flow to form aromadendrene- H^+ and higher order water clusters.

Across the flow tube from the ion source, a pinhole aperture (diameter 0.34 mm) allows a portion of the ions and neutral gas (~ 30 sccm) to flow into the mass

spectrometer, a Varian 1200 tandem mass spectrometer. The spectrometer was modified by removing the electron impact source and extending the hexapole ion guide that leads to the quadrupole mass analyzer to the pinhole aperture. For these measurements, the mass spectrometer was operated exclusively in one-dimensional mass spectrometry mode.

In order to simplify the mass spectra, a DC potential of -10 V (relative to the pinhole aperture) is applied to the hexapole. This offset pulls ions into the hexapole, where the pressure is relatively high owing to the neutral gas flow (chiefly N₂) through the pinhole. The ions therefore undergo high energy collisions with the neutral gas molecules which dissociate water clusters of analyte A:



Thus, species are predominantly observed at $m/z = M + 1$, where M is the molecular mass of the species. Hydrates, $A \cdot (H_2O)_m \cdot H^+$, particularly $m = 1$, are also observed for some species, though not for aromadendrene.

Each day, the PTR-MS sensitivity towards aromadendrene was determined by sampling standard mixtures of aromadendrene in teflon bags filled with 50 L zero air. The sensitivity was determined to be linear from 0 ppb to at least 5 ppb. Also, because of the large amounts of H₂O₂ utilized in the experiments, the sensitivity as a function of H₂O₂ was determined, with [H₂O₂] measured by operating the Varian 1200 in negative ionization mode, exploiting the reaction of CF₃O⁻ with H₂O₂ (Crouse et al., 2006). Thus, the sensitivity determined from H₂O₂-free standards was corrected for sampling from the chamber when H₂O₂ was present.

The uncertainty of aromadendrene measurements using PTR-MS is estimated to be $\sim \pm 22\%$, based on the scatter of replicate data and background measurements and uncertainties in the H_2O_2 correction.

7.9 Acknowledgements

This research was funded by U.S. Department of Energy Biological and Environmental Research Program grant DE-FG02-05ER63983. This material is based in part on work supported by the National Science Foundation under grant ATM-0432377. Alan J. Kwan acknowledged the support of NSF graduate research fellowship.

7.10 References

- Alfarra, M. R., Paulsen, D., Gysel, M., Garforth, A. A., Dommen, J., Prevot, A. S. H., Worsnop, D. R., Baltensperger, U., Coe, H.: A mass spectrometric study of secondary organic aerosols formed from the photooxidation of anthropogenic and biogenic precursors in a reaction chamber, *Atmos. Chem. Phys.*, 6, 5279-5293, 2006.
- Arey, J., Aschmann, S. M., Kwok, E. S. C., Atkinson, R.: Alkyl nitrates, hydroxyalkyl nitrates and hydroxycarbonyl formation from the NO_x – air photooxidation of C_5 - C_8 n-alkanes, *J. Phys. Chem. A*, 105, 1020-1027, 2001.
- Aschmann, S. M., Arey, J., Atkinson, R.: Atmospheric chemistry of three C_{10} alkanes. *J. Phys. Chem. A*, 105, 7598-7606, 2001.
- Aschmann, S. M., Atkinson, R., Arey, J.: Products of reaction of OH radicals with α -pinene, *J. Geophys. Res.*, 107, D14, 4191, doi: 10.1029/2001JD001098, 2002.
- Aschmann, S. M., Reissell, A., Atkinson, R., Arey, J.: Products of the gas phase reactions of the OH radical with α - and β -pinene in the presence of NO, *J. Geophys. Res.*, 103, D19, 4191, 25553-25561, 1998.
- Aschmann, S. M., Reissell, A., Atkinson, R., Arey, J.: Products of the gas phase reactions of the OH radical with a- and b-pinene in the presence of NO, *J. Geophys. Res.*, 103, D19, 25553-25561, 1998.
- Atkinson, R., Kwok, E. S. C., Arey, J., Aschmann, S. M.: Reactions of alkoxy radicals in the atmosphere, *Faraday Discuss.*, 100, 23-37, 1995.

- Atkinson, R., Arey, J.: Gas-phase tropospheric chemistry of biogenic volatile organic compounds: a review, *Atmos. Environ.*, 37, S197-S219, 2003.
- Atkinson, R., Aschmann, S. M., Winer, A. M.: Alkyl nitrate formation from the reaction of a series of branched RO₂ radicals with NO as a function of temperature and pressure, *J. Phys. Chem.*, 5, 91-102, 1987.
- Atkinson, R., Baulch, D. L., Cox, R. A., Hampson, R. F., Kerr, J. A., Rossi, M. J., Troe, J.: Evaluated kinetic and photochemical data for atmospheric chemistry, organic species, supplement VII, *J. Phys. Chem. Ref. Data.*, 28, 2, 1999.
- Atkinson, R.: Atmospheric reactions of alkoxy and β -hydroxyalkoxy radicals, *Int. J. Chem. Kinet.*, 29, 99-111, 1997a.
- Atkinson, R.: Gas phase tropospheric chemistry of organic compounds, *J. Phys. Chem. Ref. Data, Monogr, No. 2*, 11-216, 1994.
- Atkinson, R.: Gas phase tropospheric chemistry of volatile organic compounds: 1. Alkanes and Alkenes, *J. Phys. Chem. Ref. Data.*, 215-290, 1997b.
- Baldwin, A. C., Barker, J. R., Golden, D. M., Hendry, D. G.: Photochemical smog – rate parameter estimates and computer simulations, *J. Phys. Chem.*, 81, 2483-2492, 1977.
- Bahreini, R., Keywood, M. D., Ng, N. L., Varutbangkul, V., Gao, S., Flagan, R. C., Seinfeld, J. H. Measurements of secondary organic aerosol (SOA) from oxidation of cycloalkenes, terpenes, and m-xylene using an Aerodyne aerosol mass spectrometer. *Environ. Sci. Technol.*, 39, 5674-5688, 2005.
- Carreras-Sospedra, M., Griffin, R. J., Dabdub, D.: Calculations of incremental secondary organic aerosol reactivity, *Environ. Sci. Technol.*, 39, 1724-1730, 2005.
- Carter, W. P. L., Atkinson, R.: Alkyl nitrate formation from the atmospheric photooxidation of alkanes; a revised estimation, *J. Phys. Chem.*, 8, 165-173, 1989.
- Carter, W. P. L., Atkinson, R.: Atmospheric chemistry of alkanes, *J. Atmos. Chem.* 3, 377-405, 1985.
- Cocker III, D. R., Flagan, R. C., Seinfeld, J. H.: State-of-the-art chamber facility for studying atmospheric aerosol chemistry, *Environ. Sci. Technol.*, 35, 2594-2601. 2001.
- Crounse, J. D., McKinney, K. A., Kwan, A. J., Wennberg, P. O.: Measurements of gas-phase hydroperoxides by chemical ionization mass spectrometry, *Anal. Chem.*, 78, 6726-6732, 2006.

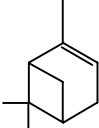
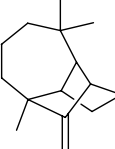
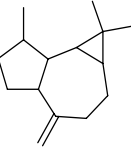
- de Gouw, J. A., Middlebrook, A. M., Warneke, C., Goldan, P. D., Kuster, W. C., Roberts, J. M., Fehsenfeld, F. C., Worsnop, D. R., Canagaratna, M. R., Pszenny, A. A. P., Keene, W. C., Marchewka, M., Bertman, S. B., and Bates, T. S.: Budget of organic carbon in a polluted atmosphere: Results from the New England Air Quality Study in 2002, *J. Geophys. Res.*, 110, D16305, doi: 10.1029/2004JD005623, 2005.
- Finlayson-Pitts, B. J., Pitts, J. N.: *Chemistry of the upper and lower atmosphere: theory, experiments and applications*, Academic Press, San Diego, 2000.
- Gao, S., Keywood, M. D., Ng, N. L., Surratt, J. D., Varutbangkul, V., Bahreini, R., Flagan, R. C. and Seinfeld, J. H.: Low-molecular weight and oligomeric components in secondary organic aerosol from the ozonolysis of cycloalkenes and α -pinene, *J. Phys. Chem. A*, 108, 10147-10164, 2004.
- Gao, S., Surratt, J. D., Kinipping, E. M., Edgerton, E. S., Shahgholi, M. Seinfeld, J. H.: Characterization of polar organic components in fine aerosols in the southeastern United States: Identity, origin, and evolution, *J. Geophys. Res.*, 111, D14314, doi:10.1029/2005JD006601, 2006.
- Geron, C., Rasmussen, R., Arnts, R. R., Guenther, A.: A review and synthesis of monoterpene speciation from forests in the United States, *Atmos. Environ.*, 34, 1761-1781, 2000.
- Glasius, M., Duane, M., Larsen, B. R.: Determination of polar terpene oxidation products in aerosols by liquid chromatography-ion trap mass spectrometry, *J. Chrom. A.*, 833, 121-135, 1999.
- Glasius, M., Lahaniati, M., Calogirou, A., Di Bella, D., Jensen, N. R., Hjorth, J., Kotzias, D., Larsen, B. R.: Carboxylic acids in secondary aerosols from oxidation of cyclic monoterpenes by ozone, *Environ. Sci. Technol.*, 34, 1001-1010, 2000.
- Griffin, R. J., Cocker, D. R., Flagan, R. C., Seinfeld, J. H., Dabdub, D.: Estimate of global atmospheric organic aerosol formation from the oxidation of biogenic hydrocarbons, *Geophys. Res. Lett.*, 26, 17, 2721-2724, 1999a.
- Griffin, R. J., Cocker, D. R., Flagan, R. C., Seinfeld, J. H.: Organic aerosol formation from the oxidation of biogenic hydrocarbons, *J. Geophys. Res.*, 104, D3, 3555-3567, 1999b.
- Guenther, A., Hewitt, C. N., Erickson, D., Fall, R., Geron, C., Graedel, T., Harley, P., Klinger, L., Lerdau, M., McKay, W. A., Pierce, T., Scholes, B., Steinbrecher, R., Tallamraju, R., Taylor, T., Zimmerman, P.: A global model of natural volatile organic compound emission, *J. Geophys. Res.*, 100, D5, 8873-8892, 1995.

- Hatakeyama, S., Izumi, K., Fukuyama, T., Akimoto, H., Washida, N.: Reactions of OH with α -pinene and β -pinene in air: Estimates of global CO production from the atmospheric oxidation of terpenes, *J. Geophys. Res.*, 96, D1, 947-958, 1991.
- Hurley, M. D., Sokolov, O., Wallington, T. J., Takekawa, H., Karasawa, M., Klotz, B., Barnes, I., Becker, K. H.: Organic aerosol formation during the atmospheric degradation of toluene, *Environ. Sci. Technol.*, 35, 1358-1366, 2001.
- Jayne, J. T., Leard, D. C., Zhang, X., Davidovits, P., Smith, K. A., Kolb, C. E., Worsnop, D. W.: Development of an Aerosol Mass Spectrometer for size and composition analysis of submicron particles, *Aerosol Sci. and Technol.*, 33, 49-70, 2000.
- Johnson, D., Jenkin, M. E., Wirtz, K., Martín-Reviejo, M. Simulating the formation of secondary organic aerosol from the photooxidation of aromatic hydrocarbons, *Environ. Chem.*, 2, 35-48, 2005.
- Johnson, D., Jenkin, M. E., Wirtz, K., Martín-Reviejo, M.: Simulating the formation of secondary organic aerosol from the photooxidation of toluene, *Environ. Chem.*, 1, 150-165, 2004.
- Kanakidou, M., Seinfeld, J. H., Pandis, S. N., Barnes, I., Dentener, F. J., Facchini, M. C., Van Dingenen, R., Evers, B., Nenes, A., Swietlicki, E., Pautaud, J. P., Balkanski, Y., Fuzzi, S., Horth, J., Moortgat, G. K., Winterhalter, R., Myhre, C. E. L., Tsigaridis, K., Vignati, E., Stephanou, E. G., Wilson, J.: Organic aerosol and global climate modeling: a review, *Atmos. Chem. Phys.*, 5, 1053-1123, 2005.
- Keywood, M. D., Varutbangkul, V., Bahreini, R., Flagan, R. C., Seinfeld, J. H.: Secondary organic aerosol formation from the ozonolysis of cycloalkenes and related compounds, *Environ. Sci. Technol.*, 38, 4157-4164, 2004.
- Klinedinst, D. B., Currie, L. A.: Direct quantification of PM_{2.5} fossil and biomass carbon within the northern front range air quality study's domain, *Environ. Sci. Technol.*, 33, 4146-4154, 1999.
- Kroll, J. H., Ng, N. L., Murphy, S. M., Flagan, R. C., Seinfeld, J. H.: Secondary organic aerosol formation from isoprene photooxidation under high-NO_x conditions, *J. Geophys. Res.*, 32, L18808, doi: 10.1029/2005GL023637, 2005.
- Kroll, J. H., Ng, N. L., Murphy, S. M., Flagan, R. C., Seinfeld, J. H.: Secondary organic aerosol formation from isoprene photooxidation, *Environ. Sci. Technol.*, 40, 1869-1877, 2006.
- Larsen, B. R., Di Bella, D., Glasius, M., Winterhalter, R., Jensen, N. R., Hjorth, J.: Gas-phase OH oxidation of monoterpenes: Gaseous and particulate products, *J. Atmos. Chem.*, 38, 2310276, 2001.

- Lim, Y. B, Ziemann, P. J.: Products and mechanism of secondary organic aerosol formation from reactions of *n*-alkanes with OH radicals in the presence of NO_x, Environ. Sci. Technol., 39, 9229-9236, 2005.
- Monod, A., Chevallier, E., Durand Jolibois, R., Doussin, J. F., Picquet-Varrault, B., Carlier, P. : Photooxidation of methylhydroperoxide and ethylhydroperoxide in the aqueous phase under simulated cloud droplet conditions, Atmos., Environ., 41, 2412-2426, 2007.
- Ng, N. L., Kroll, J. H., Keywood, M. D., Bahreini, R., Varutbangkul, V., Flagan, R. C., Seinfeld, J. H., Lee, A., and Goldstein, A. H.: Contribution of first- versus second-generation products to secondary organic aerosols formed in the oxidation of biogenic hydrocarbons, Environ. Sci. Technol., 40, 2283-2297, 2006.
- Ng, N. L., Kroll, J. H., Chan, A. W. H., Chhabra, P. S., Flagan, R. C. and Seinfeld, J. H.: Secondary organic aerosol formation from *m*-xylene, toluene, and benzene, Atmos. Chem. Phys. Discuss., 7, 4085-4126, 2007.
- O'Brien, J. M., Czuba, E., Hastie, D. R., Francisco, J. S., Shepson, P. B.: Determination of the hydroxy nitrate yields from the reaction of C₂-C₆ alkenes with OH in the presence of NO, J. Phys. Chem., 102, 8903-8908, 1998.
- Odum, J. R., Hoffmann, T., Bowman, F., Collins, D., R. C. Flagan, R. C., and Seinfeld, J. H.: Gas/particle partitioning and secondary organic aerosol yields, Environ. Sci. Technol., 30, 2580-2585, 1996.
- Odum, J. R., Jungkamp, T. P. W., Griffin, R. J., Forstner, H. J. L., Flagan, R. C., and Seinfeld, J. H.: Aromatics, reformulated gasoline and atmospheric organic aerosol formation, Environ. Sci. Technol., 31, 1890-1897, 1997.
- Owen, S. M., Boissard, C., Hewitt, C. N.: Volatile organic compounds (VOCs) emitted from 40 Mediterranean plant species: VOC speciation and extrapolation to habitat scale, Atmos. Environ., 35, 5393-5409, 2001.
- Pandis, S. N., Paulson, S. E., Seinfeld, J. H., Flagan, R. C.: Aerosol formation in the photooxidation of isoprene and β -pinene, Atmos. Environ., 25A, 997-1008, 1991.
- Presto, A. A., Huff Hartz, K. E., Donahue, N. M.: Secondary organic aerosol production from ozonolysis: 2. Effect of NO_x concentration, Environ. Sci. Technol., 39, 7046-7054, 2005.
- Seinfeld, J., Pankow, J. F.: Organic atmospheric particulate material, Annu. Rev. Phys. Chem., 54, 121-140, 2003.
- Song, C., Na, K., Cocker III, D. R.: Impact of the hydrocarbon to NO_x ratio on secondary organic aerosol formation, Environ. Sci. Technol., 39, 3143-3149, 2005.

- Sorooshian, A., Brechtel F. J., Ma, Y. L., Weber R. J., Corless, A., Flagan, R. C. and Seinfeld, J. H.: Modeling and characterization of a particle-into-liquid sampler (PILS), *Aerosol Sci. and Technol.*, 40, 396-409, 2006.
- Surratt, J. D., Kroll, J. H., Kleindienst, T. E., Edney, E. O., Claeys, M., Sorooshian, A., Ng, N. L., Offenberg, J. H., Lewandowski, M., Jaoui, M., Flagan, R. C. and Seinfeld, J. H.: Evidence for organosulfates in secondary organic aerosol, *Environ. Sci. Technol.*, 41, 517-527, 2007.
- Surratt, J. D., Murphy, S. M., Kroll, J. H., Ng, N. L., Hildebrandt, L., Sorooshian, A., Szmigielski, R., Vermeylen, R., Maenhaut, W., Claeys, M., Flagan, R. C. and Seinfeld, J. H.: Chemical composition of secondary organic aerosol formed from the photooxidation of isoprene, *J. Atmos. Chem.*, 31, 9665-9690, 2006.
- Szmigielski, R., Surratt, J. D., Vermeylen, R., Szmigielska, K., Kroll, J. H., Ng, N. L., Murphy, S. M., Sorooshian, A., Seinfeld, J. H., Claeys, M.: Characterization of 2-methylglyceric acid oligomers in secondary organic aerosol formed from the photooxidation of isoprene using trimethylsilylation and gas chromatography/ion trap mass spectrometry, *J. Mass Spectrom.*, 42, 101-116, 2007.
- Talukar, R. K., Herndon, S. C., Burkholder, J. B., Roberts, J. M., Ravishankara, A. R.: Atmospheric fate of several alkyl nitrates, *J. Chem. Soc., Faraday Trans.*, 93, 2787-2796, 1997.
- Treves, K., Rudich, Y.: The atmospheric fate of C₃-C₆ hydroxyalkyl nitrates, *J. Phys. Chem. A*, 107, 7809-7817, 2003.
- Zhang, J., Dransfield, T., Donahue, N. M.: On the mechanism for nitrate formation via the peroxy radical + NO reaction, *J. Phys. Chem. A*, 108, 9082-9095, 2004.
- Zhang, J., Hartz, K. E. H., Pandis, S. N., and Dohanue, N. M.: Secondary organic aerosol formation from limonene ozonolysis: Homogeneous and heterogeneous influences as a function of NO_x, *J. Phys. Chem., A*, 110, 11053-11063, 2006.
- Zhang, S. H., Shaw, M., Seinfeld, J. H., Flagan, R. C.: Photochemical aerosol formation from α -pinene and β -pinene, *J. Geophys. Res.*, 97, D18, 20717-20729, 1992.

Table 7. 1. Parent hydrocarbons studied

Parent Hydrocarbon	Structure	Formula (MW)	k_{OH} ($\text{cm}^3 \text{ molec}^{-1} \text{ s}^{-1}$)
α -pinene		$\text{C}_{10}\text{H}_{16}$ (136)	$5.3 \times 10^{-11} \text{ a}$
longifolene		$\text{C}_{15}\text{H}_{24}$ (204)	$4.8 \times 10^{-11} \text{ a}$
aromadendrene		$\text{C}_{15}\text{H}_{24}$ (204)	$1.5 \times 10^{-10} \text{ b}$

a: Rate constants were obtained from Atkinson et al. (2003)

b: Rate constant was estimated from the rate of aromadendrene decay (experiment 1 in Table 7.4), assuming an OH concentration of $3 \times 10^6 \text{ molecule cm}^{-3}$ and that aromadendrene reacts with OH only

Table 7. 2. Initial conditions and data for α -pinene experiments

Expt. No.	NO _x Condition	NO (ppb)	NO ₂ (ppb)	T (K)	RH (%)	Δ H _C (ppb) ^a	Δ M ₀ (μ g/m ³) ^b	SOA Yield (%) ^c
1	H ₂ O ₂	0	0	298	5.3	13.8 \pm 0.2	29.3 \pm 2.4	37.9 \pm 3.2
2	H ₂ O ₂	0	1	298	6.2	47.5 \pm 0.8	121.3 \pm 9.4	45.8 \pm 3.6
3	H ₂ O ₂ + NO	198	0	296	6.4	13.1 \pm 0.2	15.6 \pm 1.4	21.2 \pm 2.0
4	HONO	475	463	299	3.3	12.6 \pm 0.2	4.5 \pm 0.9	6.6 \pm 1.4
5	HONO	390	578	298	3.7	46.6 \pm 0.8	40.8 \pm 3.8	15.8 \pm 1.5

a: Stated uncertainties include scatter in GC measurements and GC calibration errors

b: Stated uncertainties are from scatter in particle volume measurements

c: Stated uncertainties are propagated from errors in Δ H_C and Δ M₀

Table 7. 3. Initial conditions and data for longifolene experiments

Expt. No.	NO _x Condition	NO (ppb)	NO ₂ (ppb)	T (K)	RH (%)	ΔHC (ppb) ^b	ΔM _o (μg/m ³) ^c	SOA Yield (%) ^d
1	H ₂ O ₂	0	0	298	5.8	4.5 ± 0.2	28.5 ± 2.4	75.7 ± 7.0
2	H ₂ O ₂	0	2	297	6.0	8.4 ± 0.4	52.5 ± 4.2	74.4 ± 6.7
3	H ₂ O ₂	0	2	297	6.3	19.4 ± 0.8	117.1 ± 9.3	72.1 ± 6.5
4	H ₂ O ₂	0	2	299	5.7	24.8 ± 1.1	148.4 ± 11.6	71.8 ± 6.4
5	H ₂ O ₂ + NO	70	31 ^a	297	6.2	3.8 ± 0.2	35.8 ± 2.9	111.7 ± 10.2
6	H ₂ O ₂ + NO	209	26 ^a	297	8.0	4.7 ± 0.2	43.4 ± 3.5	110.2 ± 10.0
7	H ₂ O ₂ + NO	316	0	298	6.4	4.1 ± 0.2	43.4 ± 3.5	127.2 ± 11.5
8	H ₂ O ₂ + NO	394	0	297	6.1	4.8 ± 0.2	50.0 ± 4.1	124.9 ± 11.5
9	H ₂ O ₂ + NO	564	0	297	6.2	3.9 ± 0.2	51.6 ± 4.1	157.0 ± 14.1
10	HONO	428	550	298	3.7	9.7 ± 0.4	68.3 ± 5.1	84.0 ± 7.1
11	HONO	469	502	298	3.7	19.6 ± 0.9	141.9 ± 10.3	86.8 ± 7.3
12	HONO	394	577	299	3.2	26.6 ± 1.2	213.6 ± 15.3	96.3 ± 8.0

a: NO₂ formed due to NO reacting with residual ozone in the chamber

b: Stated uncertainties include scatter in GC measurements and GC calibration errors

c: Stated uncertainties are from scatter in particle volume measurements

d: Stated uncertainties are propagated from errors in ΔHC and ΔM_o

Table 7. 4. Initial conditions and data for aromadendrene experiments

Expt. No.	NO _x Condition	NO (ppb)	NO ₂ (ppb)	T (K)	RH (%)	ΔHC (ppb) ^a	ΔM ₀ (μg/m ³) ^b	SOA Yield (%)
1	H ₂ O ₂	0	0	299	5.5	5.7 ± 1.2	19.7 ± 2.0	41.7 ± 10
2	H ₂ O ₂ + NO	120	0	298	9.3	5.3 ± 1.2	23.1 ± 2.2	52.0 ± 12.4
3	H ₂ O ₂ + NO	195	0	298	7.7	6.0 ± 1.4	29.3 ± 2.6	58.8 ± 14.4
4	H ₂ O ₂ + NO	517	0	299	7.4	3.2 ± 0.7	22.6 ± 2.2	84.7 ± 20.0

a: Stated uncertainties include scatter in CIMS measurements and CIMS calibration errors

b: Stated uncertainties are from scatter in particle volume measurements

Table 7. 5. Estimated effective SOA densities

Parent Hydrocarbon	NO _x Condition	Effective Density (g cm ⁻³) ^a
α-pinene	H ₂ O ₂	1.32 ± 0.10
α-pinene	H ₂ O ₂ + NO	1.32 ± 0.10
α-pinene	HONO	1.33 ± 0.10
longifolene	H ₂ O ₂	1.29 ± 0.10
longifolene	H ₂ O ₂ + NO	1.30 ± 0.10
longifolene	HONO	1.40 ± 0.10
aromadendrene	H ₂ O ₂	1.20 ± 0.10
aromadendrene	H ₂ O ₂ + NO	1.35 ± 0.10

a: Stated uncertainties (1σ) are from repeated measurements of ammonium sulfate seed densities

Table 7. 6. α -Pinene acidic SOA components detected by the UPLC/ESI-TOFMS instrument

Experiment	Measured [M - H] ⁻ ion (<i>m/z</i>)	TOFMS suggested molecular formula	Error (mDa)	Error (ppm)	Retention Time
H ₂ O ₂	157.0497	C ₇ H ₉ O ₄ ⁻	-0.4	-2.5	5.09
	169.0873	C ₉ H ₁₃ O ₃ ⁻	0.8	4.7	6.89
	171.0654	C ₈ H ₁₁ O ₄ ⁻	-0.3	-1.8	5.61
	183.1027	C ₁₀ H ₁₅ O ₃ ⁻	0.6	3.3	7.50
	185.0821	C ₉ H ₁₃ O ₄ ⁻	0.7	3.8	6.85
	199.0983	C ₁₀ H ₁₅ O ₄ ⁻	1.3	6.5	6.17
	199.0982	C ₁₀ H ₁₅ O ₄ ⁻	1.2	6.0	6.29
	199.0976	C ₁₀ H ₁₅ O ₄ ⁻	0.6	3.0	6.34
	215.0923	C ₁₀ H ₁₅ O ₅ ⁻	0.4	1.9	5.99
	215.0930	C ₁₀ H ₁₅ O ₅ ⁻	1.1	5.1	7.18
	231.0885	C ₁₀ H ₁₅ O ₆ ⁻	1.6	6.9	6.80
H ₂ O ₂ + NO	157.0499	C ₇ H ₉ O ₄ ⁻	-0.2	-1.3	5.08
	171.0655	C ₈ H ₁₁ O ₄ ⁻	-0.2	-1.2	5.60
	183.1025	C ₁₀ H ₁₅ O ₃ ⁻	0.4	2.2	7.49
	185.0812	C ₉ H ₁₃ O ₄ ⁻	-0.2	-1.1	6.86
	197.0814	C ₁₀ H ₁₃ O ₄ ⁻	0.0	0.0	8.09
	199.0971	C ₁₀ H ₁₅ O ₄ ⁻	0.1	0.5	6.36
	203.0557	C ₈ H ₁₁ O ₆ ⁻	0.1	0.5	5.50
	215.0925	C ₁₀ H ₁₅ O ₅ ⁻	0.6	2.8	6.23
	229.0718	C ₁₀ H ₁₃ O ₆ ⁻	0.6	2.6	6.17
231.0856	C ₁₀ H ₁₅ O ₆ ⁻	-1.3	-5.6	6.79	
HONO	171.0649	C ₈ H ₁₁ O ₄ ⁻	-0.8	-4.7	5.60
	183.1022	C ₁₀ H ₁₅ O ₃ ⁻	0.1	0.5	7.49
	185.0457	C ₈ H ₉ O ₅ ⁻	0.7	3.8	6.63
	187.0606	C ₈ H ₁₁ O ₅ ⁻	0.0	0.0	5.65
	197.0819	C ₁₀ H ₁₃ O ₄ ⁻	0.5	2.5	8.09
	203.0546	C ₈ H ₁₁ O ₆ ⁻	-1.0	-4.9	5.50
	213.0781	C ₁₀ H ₁₃ O ₅ ⁻	1.8	8.4	5.26
	231.0883	C ₁₀ H ₁₅ O ₆ ⁻	1.4	6.1	6.80
	259.1182	C ₁₂ H ₁₉ O ₆ ⁻	0.0	0.0	5.85
	322.1148	C ₁₂ H ₂₀ NO ₉ ⁻	1.0	3.1	7.62

Table 7. 7. Longifolene SOA components detected by the UPLC/ESI-TOFMS instrument

Experiment	Measured [M - H] ⁻ ion (m/z)	TOFMS suggested molecular formula	Error (mDa)	Error (ppm)	Retention Time (min)
H ₂ O ₂	223.1344	C ₁₃ H ₁₉ O ₃ ⁻	1.0	4.5	8.92
	237.1500	C ₁₄ H ₂₁ O ₃ ⁻	0.9	3.8	9.06
	239.1651	C ₁₄ H ₂₃ O ₃ ⁻	0.4	1.7	10.50
	253.1445	C ₁₄ H ₂₁ O ₄ ⁻	0.5	2.0	9.36
	249.1499	C ₁₅ H ₂₁ O ₄ ⁻	0.8	3.2	9.25
	249.1501	C ₁₅ H ₂₁ O ₄ ⁻	1.0	4.0	10.14
	255.1611	C ₁₄ H ₂₃ O ₄ ⁻	1.5	5.9	9.88
	255.1622	C ₁₄ H ₂₃ O ₄ ⁻	2.6	10.2	8.99
	267.1602	C ₁₅ H ₂₃ O ₄ ⁻	0.6	2.2	8.88
	267.1606	C ₁₅ H ₂₃ O ₄ ⁻	1.0	3.7	9.01
	267.1611	C ₁₅ H ₂₃ O ₄ ⁻	1.5	5.6	9.28
	267.1601	C ₁₅ H ₂₃ O ₄ ⁻	0.5	1.9	9.70
	269.1392	C ₁₄ H ₂₁ O ₅ ⁻	0.3	1.1	7.71
	283.1561	C ₁₅ H ₂₃ O ₅ ⁻	1.6	5.7	7.35
	313.2018	C ₁₇ H ₂₉ O ₅ ⁻	0.3	1.0	9.20
	H ₂ O ₂ + NO	223.1337	C ₁₃ H ₁₉ O ₃ ⁻	0.3	1.3
239.1649		C ₁₄ H ₂₃ O ₃ ⁻	0.2	0.8	10.49
265.1442		C ₁₅ H ₂₁ O ₄ ⁻	0.2	0.8	8.93
269.1401		C ₁₄ H ₂₁ O ₅ ⁻	1.2	4.5	7.72
316.1396		C ₁₄ H ₂₂ NO ₇ ⁻	0.0	0.0	9.88
329.1972		C ₁₇ H ₂₉ O ₆ ⁻	0.8	2.4	9.35
372.1664		C ₁₇ H ₂₆ NO ₈ ⁻	0.6	1.6	10.58
374.1829		C ₁₇ H ₂₈ NO ₈ ⁻	1.4	3.7	9.14
374.1829		C ₁₇ H ₂₈ NO ₈ ⁻	1.4	3.7	9.35
390.1775		C ₁₇ H ₂₈ NO ₉ ⁻	1.1	2.8	9.46
HONO	223.1334	C ₁₃ H ₁₉ O ₃ ⁻	-0.1	-0.4	8.92
	241.1453	C ₁₃ H ₂₁ O ₄ ⁻	1.3	5.4	7.55
	253.1431	C ₁₄ H ₂₁ O ₄ ⁻	-0.9	-3.6	8.02
	269.1394	C ₁₄ H ₂₁ O ₅ ⁻	0.5	1.9	7.18
	269.1408	C ₁₄ H ₂₁ O ₅ ⁻	1.9	7.1	7.71
	342.1930	C ₁₇ H ₂₈ NO ₆ ⁻	1.3	3.8	9.65
	344.1348	C ₁₅ H ₂₂ NO ₈ ⁻	0.3	0.9	8.25
	346.1502	C ₁₅ H ₂₄ NO ₈ ⁻	0.2	0.6	8.34
	360.1674	C ₁₆ H ₂₆ NO ₈ ⁻	1.6	4.4	8.89
	372.1667	C ₁₇ H ₂₆ NO ₈ ⁻	-0.6	-1.6	10.61
	374.1809	C ₁₇ H ₂₈ NO ₈ ⁻	-0.6	-1.6	8.89
	374.1816	C ₁₇ H ₂₈ NO ₈ ⁻	0.1	0.3	9.13
	374.1808	C ₁₇ H ₂₈ NO ₈ ⁻	-0.7	-1.9	9.35
	390.1773	C ₁₇ H ₂₈ NO ₉ ⁻	0.9	2.3	8.49
	390.1778	C ₁₇ H ₂₈ NO ₉ ⁻	1.4	3.6	9.21
435.1619	C ₁₇ H ₂₇ N ₂ O ₁₁ ⁻	0.4	0.9	9.56	

Figure 7. 1. Time-dependent growth curves for α -pinene photooxidation under different NO_x conditions.

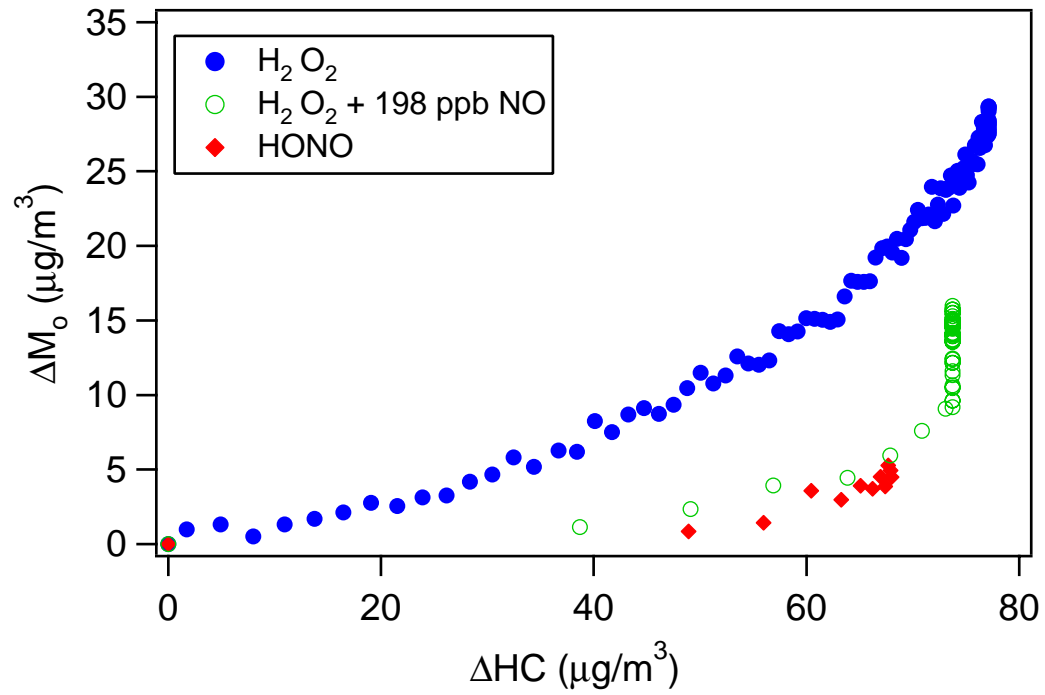


Figure 7. 2. Time-dependent growth curves for longifolene photooxidation under high- and low- NO_x conditions. The mixing ratios in the legend refer to the amount of longifolene reacted in each experiment.

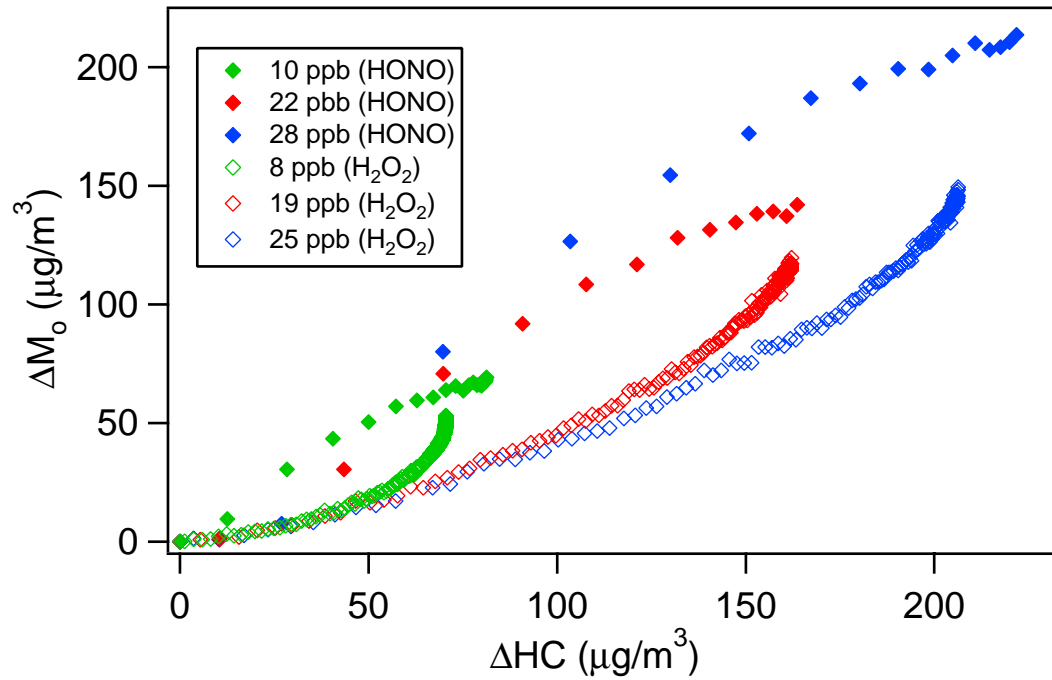


Figure 7. 3. Time-dependent growth curves for longifolene photooxidation with H_2O_2 as an OH precursor. Aerosol growth in the presence of ~ 300 ppb NO (Experiment 7 in Table 7.3) exceeds that without NO.

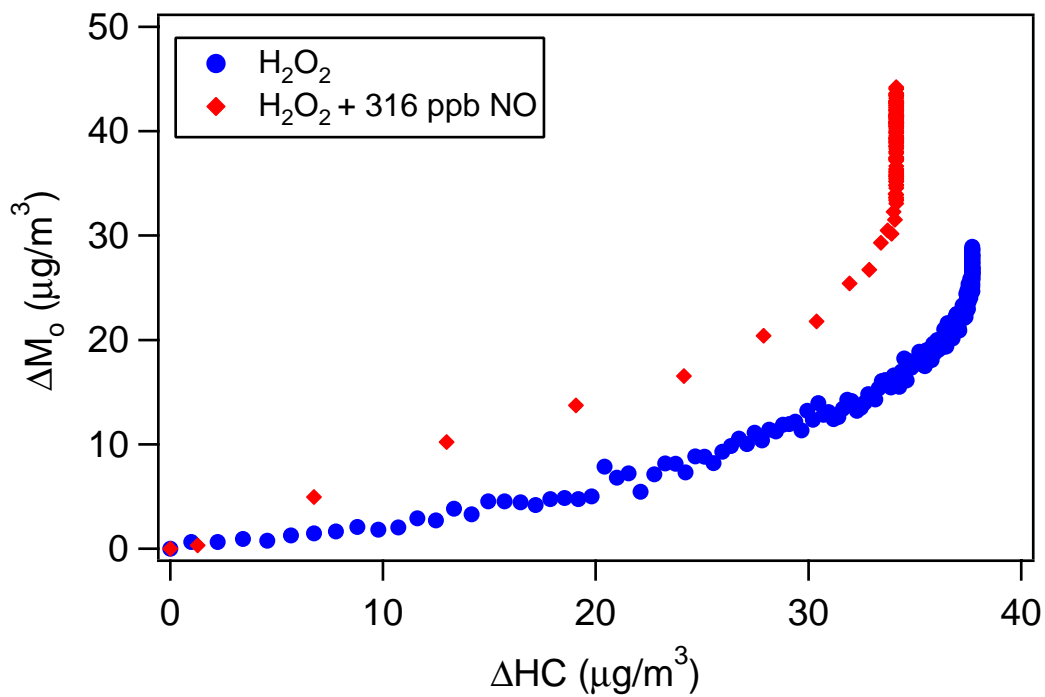


Figure 7. 4. SOA growth as a function of initial NO_x concentrations, for a fixed longifolene concentration (~ 4.3 ppb). Results shown are from Table 7.3.

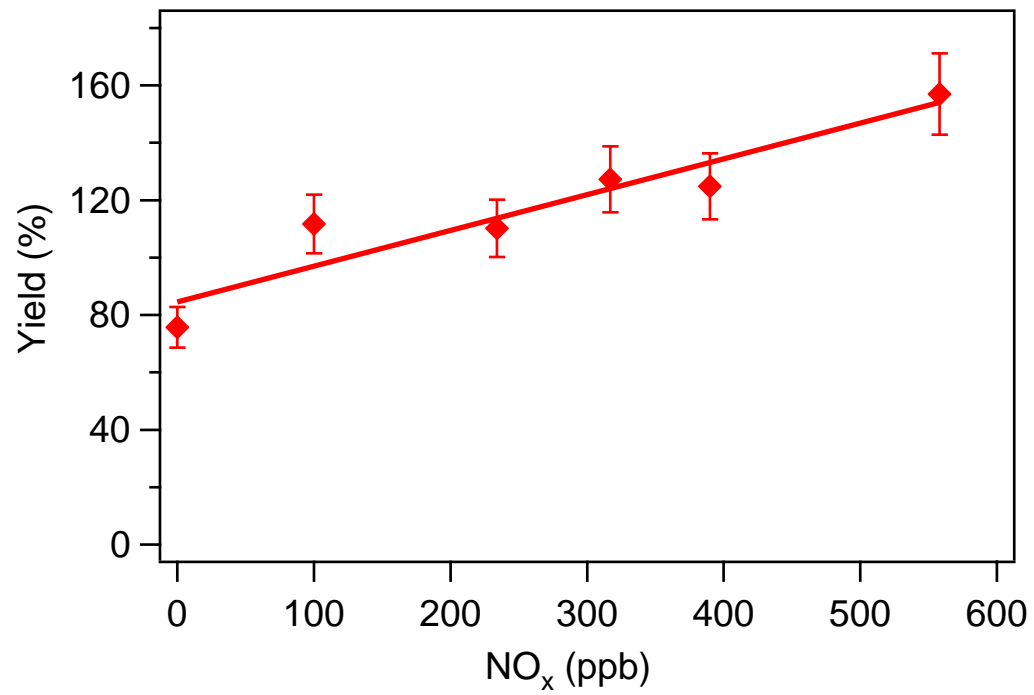


Figure 7. 5. SOA growth as a function of initial NO_x concentration, at a fixed initial aromadendrene concentration (~ 5 ppb). Results shown are from Table 7.4.

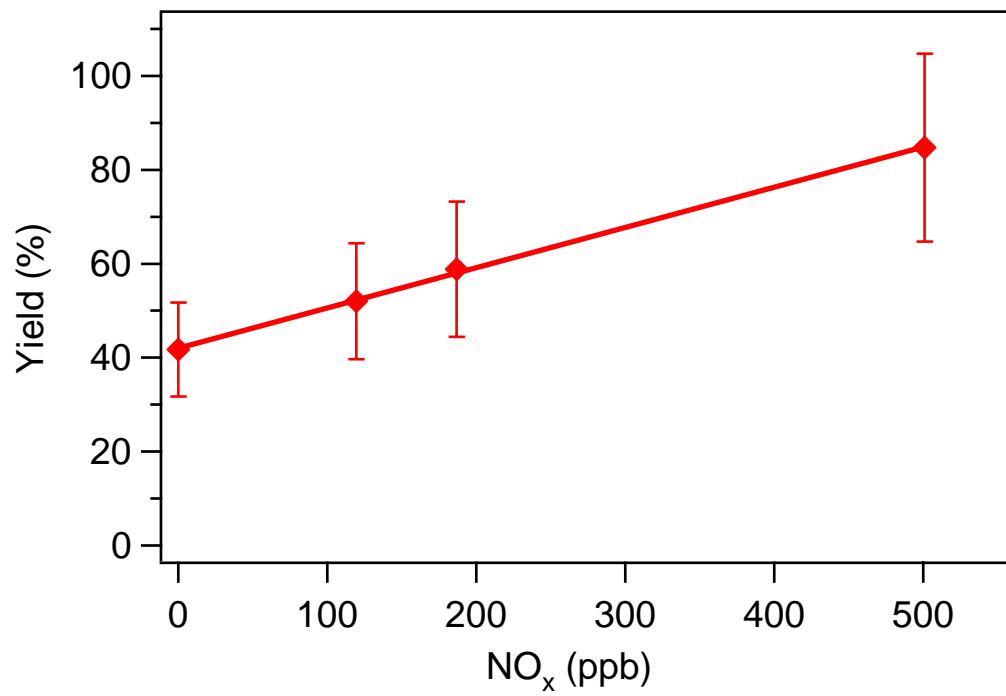


Figure 7. 6. AMS high-NO_x spectra signal versus low-NO_x spectra signal for α -pinene photooxidation. Each mass fragment is normalized by the total signal. The solid black line is the one-to-one line. The spectra are taken when all hydrocarbon has been consumed.

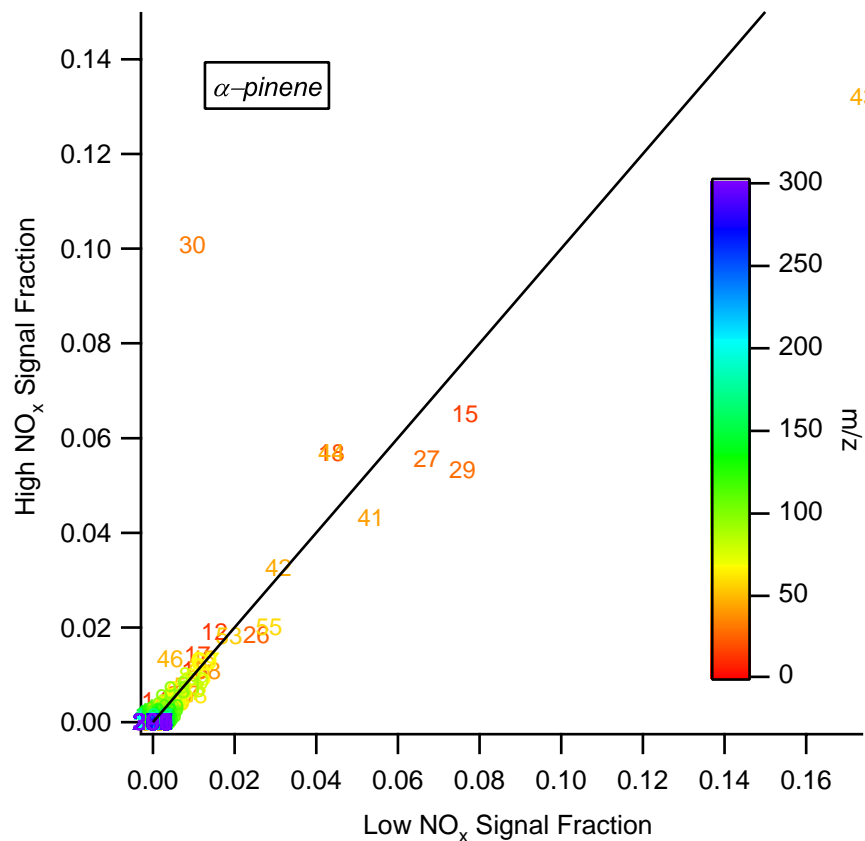


Figure 7. 7. AMS high-NO_x spectra signal versus low-NO_x spectra signal for longifolene photooxidation. Each mass fragment is normalized by the total signal. The solid black line is the 1:1 line. The spectra are taken when all hydrocarbon has been consumed.

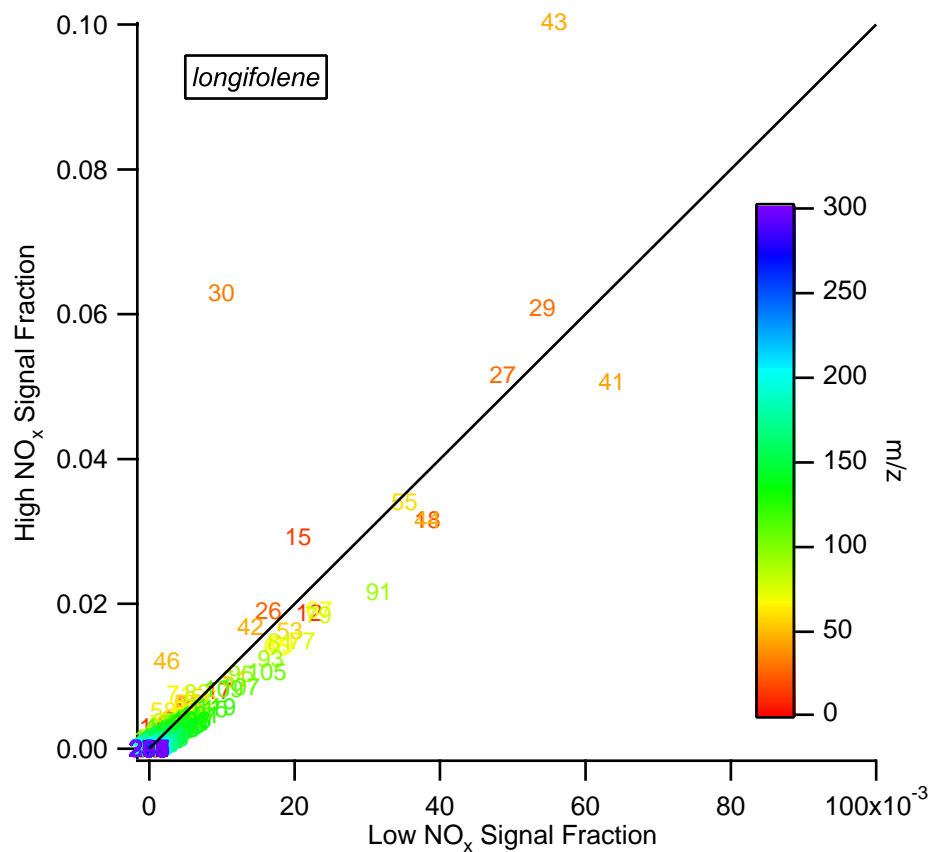


Figure 7. 8. Ratio of the sum of masses at m/z 30 and 46 to total organic mass as a function of organic mass as measured by the AMS for α -pinene photooxidation. The higher ratio for high- NO_x experiments suggests the formation of nitrate species.

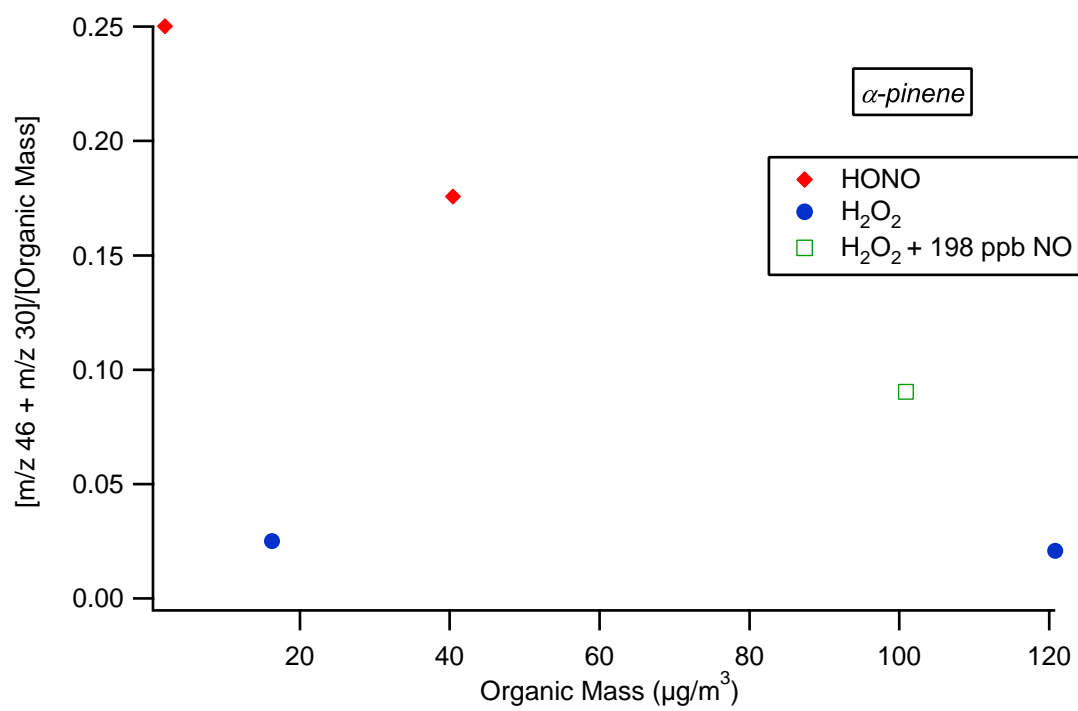


Figure 7. 9. Ratio of the sum of masses at m/z 30 and 46 to total organic mass as a function of organic mass as measured by the AMS for longifolene photooxidation. The higher ratio for high- NO_x experiments suggests the formation of nitrate species.

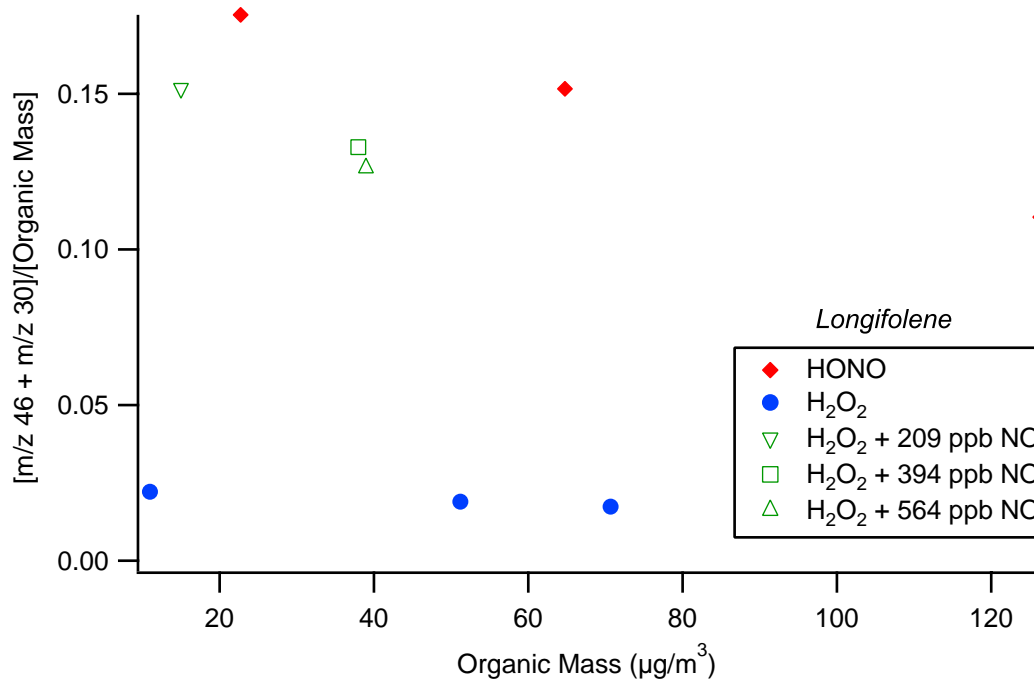


Figure 7. 10. Changes in AMS spectrum over the course of longifolene photooxidation under high- NO_x conditions. Top panel: Fractional contribution of each mass fragment to the total organic and nitrate signal during the growth phase of the experiment. Bottom panel: Percentage change of each mass fragment from the growth phase to the point at which all of the hydrocarbon is consumed.

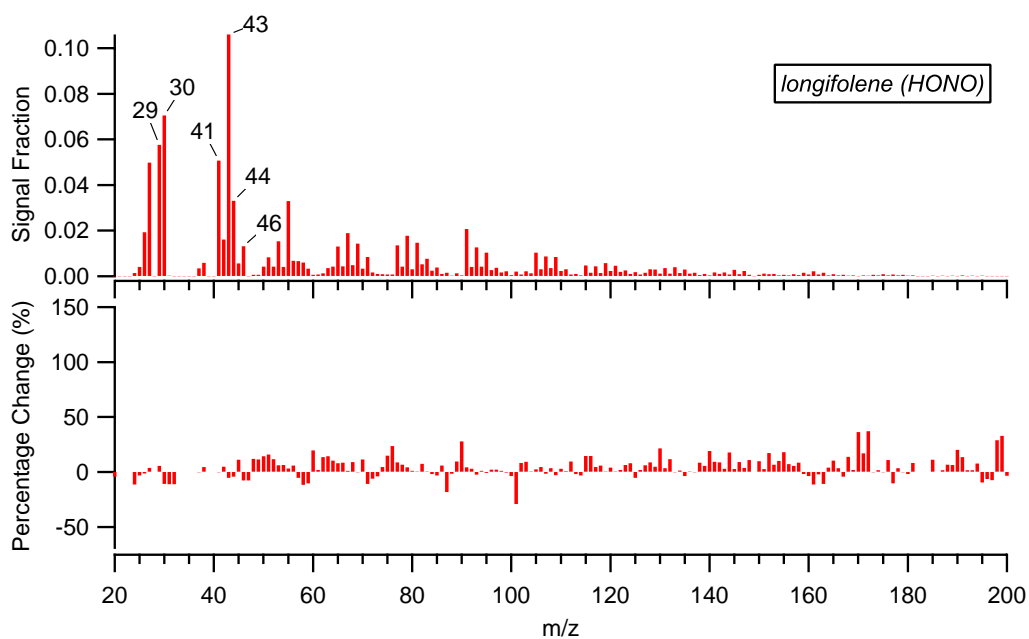


Figure 7. 11. Changes in AMS spectrum over the course of longifolene photooxidation under low-NO_x conditions. Top panel: Fractional contribution of each mass fragment to the total organic and nitrate signal during the growth phase of the experiment. Bottom panel: Percentage change of each mass fragment from the growth phase to the point at which all of the hydrocarbon is consumed.

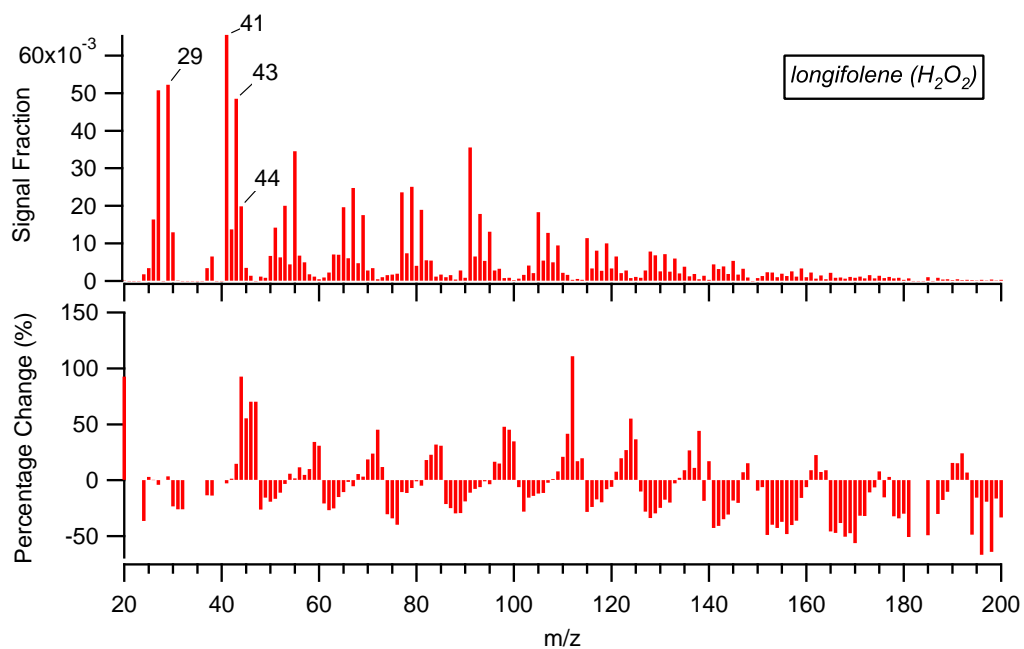


Figure 7. 12. UPLC/ESI-TOFMS extracted ion chromatograms (EICs) ($= m/z$ 346 + 374 + 390) for longifolene photooxidation experiments. The even $[M - H]^-$ ions listed above the chromatographic peaks correspond to organic nitrates detected in longifolene SOA. No organic nitrates are detected in the H_2O_2 experiment. The HONO experiment has the widest array of organic nitrates detected (as shown in Table 7.7), as well as the largest chromatographic peaks; m/z 372 is the only exception, and is most abundant in the " $H_2O_2 + NO$ " experiment. These EICs are directly comparable as the volume of chamber air sampled is approximately the same (2 m^3).

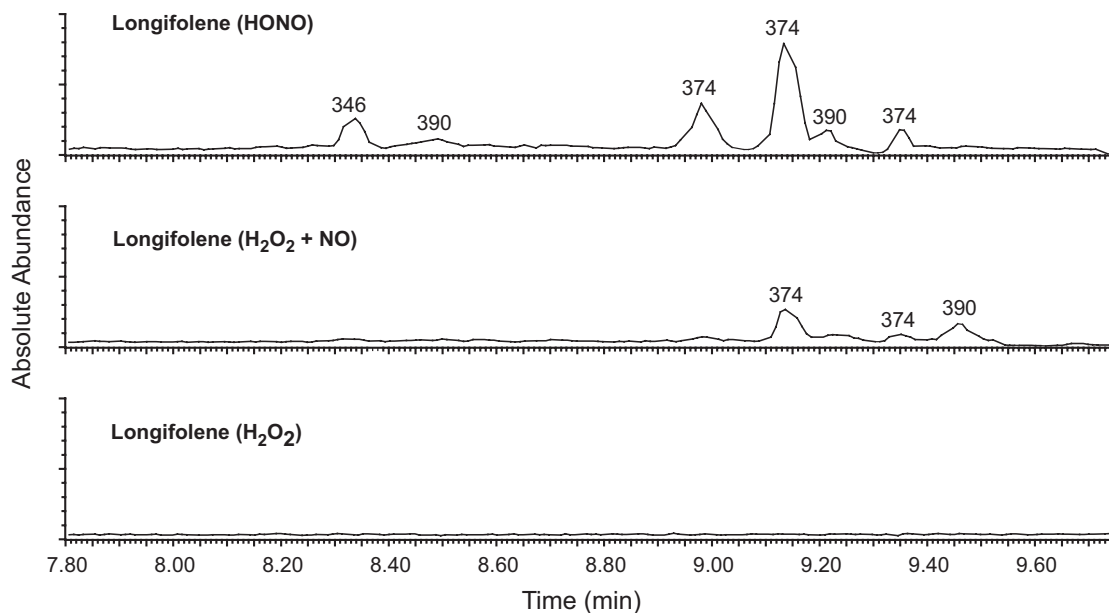


Figure 7. 13. General schematic of gas-phase peroxy radical chemistry in SOA formation.

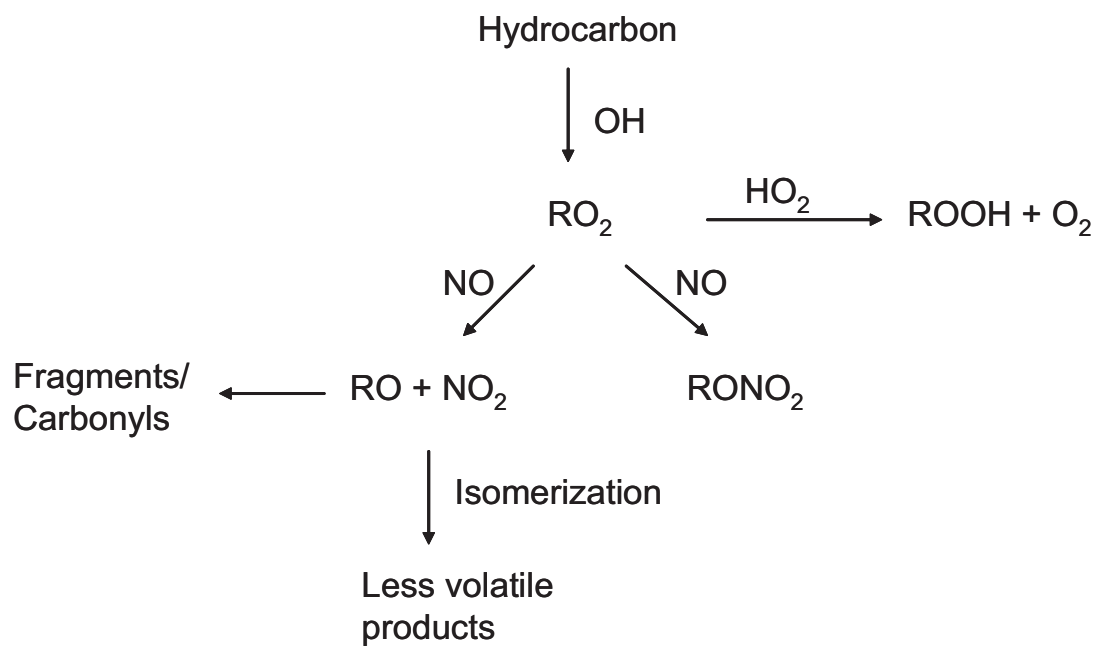


Figure 7. 14. A kinetic scheme depicting the competition between gas-particle partitioning and irreversible loss of the gas-phase semivolatiles. X represents the product of generic loss of semivolatile species A_g by chemical reaction, and/or loss to chamber walls. k' is the pseudo-first-order rate constant ($k' = k_{OH}[OH]$) for photooxidation of the parent hydrocarbon; k_g is the first-order rate constant of loss of semivolatiles.

